Factors Controlling the Decomposition of Ectomycorrhizal Fungal Tissue and the Formation of Soil Organic Matter

A Thesis

SUBMITTED TO THE FACULTY OF THE

UNIVERSITY OF MINNESOTA

BY

Maeve Elizabeth Ryan

IN PARTIAL FULFILLMENT OF THE REQUIREMENTS

FOR THE DEGREE OF

MASTER OF SCIENCE

Kathryn M. Schreiner, Advisor

JUNE 2019

Acknowledgements

Several people have played important roles in my research and overall graduate experience and deserve to be acknowledged. First, my research adviser, Dr. Kathryn Schreiner, has provided so much support throughout the nearly two years I have worked in her lab and always challenged me to take my research one step further. She devoted a lot of time and energy to this project and this document and it wouldn't be where it is without her. Dr. Liz Minor and Dr. Peter Kennedy have provided valuable input as committee members and helped guide this research. I would like to thank the Kennedy lab for generating necromass and organizing the degradation study, and specifically Joe Gagne and Amanda Certano for their help on burial day. I would like to thank Cedar Creek Ecosystem Science Reserve and the Long-Term Ecological Research Program (LTER) for the use of their land to conduct this degradation study. I would also like to acknowledge Julie Halbur for keeping the lab running and for her patience in teaching me to maintain the instruments myself. I would like to acknowledge Dr. Erin Sheets for the use of her lab space and equipment for the melanin isolations and for her help optimizing the isolation protocol, as well as Dr. Melissa Maurer-Jones for allowing us to use her FTIR.

The other members of the Schreiner group gave me support and feedback during my time in the group. Val Bruner set up the groundwork for the methods used in this research and assembled the compound library used for peak classification. Jenna Swenson was an integral part of this project: she trekked back and forth to the field site with me, helped prepare the samples back in lab, and provided endless moral support, in addition to running and analyzing FTIR of the fungal species collected.

I would like to thank the University of Minnesota Duluth Department of Chemistry and Biochemistry for their support throughout this process, including funding through teaching assistantships and the Cothran Memorial Fellowship. I am grateful for the valuable support I have received from my fellow graduate students, especially my roommates, Alvin Burrows and Daniel Zoltek. Lastly, I want to thank my parents, Joe and Dee Ryan, and my brother, Garrett Ryan, for their support through my graduate degree and before.

ABSTRACT

The turnover of ectomycorrhizal (ECM) fungi accounts for up to half of the organic carbon found in forest soils and therefore represents an important pathway for the removal of carbon from the atmosphere to be stored belowground as long-lived soil organic matter (SOM). Understanding the flux of fungal necromass inputs to SOM, and their subsequent stabilization potential in forest soils, requires an understanding of the chemical changes that occur during the degradation of fungal tissue. Additionally, it is hypothesized that degradation of fungal necromass is slowed by high melanin content and accelerated by high nitrogen content. A field degradation study was carried out at the Cedar Creek Ecosystem Science Reserve in East Bethel, Minnesota. Necromass from four species of ECM fungi with varying degrees of melanization was buried in litter bags in a *Pinus*-dominated forest below the soil litter layer, allowed to degrade naturally, and harvested nine times over a period of 90 days. Harvest was more frequent during the first week to gain insight into the dynamic early decomposition period. Elemental analysis (EA), Fourier-transform infrared spectroscopy (FTIR), and thermochemolysis-gas chromatography-mass spectrometry (pyGCMS), including novel methods of quantifying the contribution from various types of biopolymers to the total remaining tissue, supplement mass loss data to provide an overview of the chemical changes that occur as fungal necromass decomposes. Each of the four species lost a significant amount of mass in the first seven days of incubation but, at the end of the three-month degradation sequence, a significant fraction of fungal necromass remained. This necromass was chemically distinct from undegraded necromass, containing more aromatic compounds, suggesting that the relative abundance of melanin, which is highly aromatic, increased as other cellular components degraded away. Although melanin content was hypothesized to slow degradation, a high-melanin species degraded at effectively the same rate as the two low-melanin species. Differences in degradation rates across species can be attributed to initial nitrogen content, while melanin content could explain differences in degradation rate within a species.

Table of Contents

List of Tables

List of Figures

CHAPTER 1. LITERATURE REVIEW

1.1 Global carbon cycling

There is about 40 x 10^{18} g of carbon at or near Earth's surface engaging in the global carbon cycle (Schlesinger & Bernhardt, 2013). This carbon is found in soils, biomass, water, and the atmosphere. Physical and biological processes control the movement of carbon throughout these reservoirs. For example, carbon is transported from the atmosphere to plant biomass through photosynthesis, to water through erosion and dissolution, and carbon dioxide re-enters the atmosphere through respiration. The carbon cycle has been altered anthropogenically in many ways, for example through the combustion of fossil fuels and deforestation.

Soils store a large amount of organic carbon that has been removed from the atmosphere and therefore from the fast-cycling biological carbon cycle, which consists of photosynthesis and respiration by plants and heterotrophs. Twice as much carbon is stored in soil organic matter (SOM) globally as exists as carbon dioxide in the atmosphere, totaling an estimated 1500 Pg in the top meter of soil (Jobbágy & Jackson, 2000). As long as this store of carbon remains stable, soil will continue to be a major carbon sink. Degradation of SOM, though, has the potential to convert soil into a carbon source if SOM is degraded to carbon dioxide or methane and respired into the atmosphere.

Global climate changes, such as increased temperature from increased levels of carbon dioxide in the atmosphere, affect the decomposition of SOM, but how and to what extent remain unclear (Conant et al., 2011). Increased temperature and carbon dioxide can initiate a positive or negative feedback loop in terms of soil respiration. In a positive feedback loop, increased temperature leads to increased degradation of soil organic matter

which causes more carbon dioxide to be respired into the atmosphere, thereby exacerbating climate change (Davidson and Janssens, 2006). In the case of a negative feedback loop, the amount of carbon respired into the atmosphere is outweighed by an increase in carbon allocated belowground (Davidson and Janssens, 2006). This occurs because elevated carbon dioxide levels induce photosynthesis and suppress respiration (Drake et al., 1997) and therefore plants have more carbon to allocate belowground. Therefore, elevated temperature has complex effects on photosynthesis and respiration which could either increase or decrease soil carbon storage (Dusenge et al., 2018). If the amount of carbon allocated belowground exceeds the amount respired into the atmosphere, there would be a net increase in soil carbon storage (Davidson and Janssens, 2006). In addition, land use change has decreased the amount of SOM and is responsible for approximately one third of the 3.5 Pg of carbon released from soil annually (Lal, 2004; Ontl & Schulte, 2012). Cultivation of land for agriculture, for example, leads to a decrease in SOM by exposing more soil to moisture and oxygen, breaking up soil aggregates that had been physically protecting SOM, and introducing more readily decomposed tissue to the soil, thereby increasing the rate of decomposition of SOM through priming effects (Post and Kwon, 2000). How, and to what extent, climate and land use changes will affect the carbon cycle in the future remains uncertain.

1.2 Soil organic matter chemistry

Long-lived SOM is composed of stable organic compounds, including fragments from lignin, polysaccharides, polyphenols, lipids, and other biomolecules (Kallenbach et al., 2016). It originates from both above- and belowground sources. Until recently,

aboveground litterfall from plants was thought to contribute the majority of organic matter to SOM (Swift, 1979). However, evidence gathered in recent years suggests that belowground inputs of carbon contribute more to SOM than previously thought. In fact, it was shown that up to 70% of the carbon in forest soils originates from belowground sources such as plant roots and soil fungi (Clemmensen et al., 2013). It has been demonstrated that soil microbes themselves can contribute carbon to longer-lived SOM, and that degradation-resistant SOM looks more like microbial products than plant products on a molecular level (Kallenbach et al., 2016; Simpson et al., 2007).

The turnover of soil fungi has gained recognition as a major input of carbon into soil, contributing to the long-term accumulation of SOM (Godbold et al., 2006; Kögel-Knabner, 2002). The relative abundance of fungus in soil varies, mainly in response to soil disturbance (Six et al., 2006). One study, though, showed that ectomycorrhizal fungus accounts for about one third of soil microbial biomass (Högberg and Högberg, 2002). In addition, mycorrhizal fungi have been shown to contribute more than half of the total carbon found in SOM, totaling more than leaf litter and fine root turnover combined (Godbold et al., 2006). The chemical similarities between microbial-derived organic matter and SOM, in addition to the demonstrated retention of microbial-derived organic matter in soils, suggest that fungi play a more important role in soil carbon storage than previously assumed.

Traditionally, the rate of SOM degradation has been thought to depend solely on the biochemical "quality" of the organic matter, especially the ratio of carbon to nitrogen in the SOM (Swift, 1979). Organic matter high in nitrogen tends to be degraded more rapidly than organic matter low in nitrogen because nitrogen is a valuable nutrient and

therefore desirable to decomposers. This trend has been demonstrated in birch leaf litter (Cotrufo et al., 1995), litter from conifers and hardwoods (Taylor et al., 1989), and fungal necromass (Koide & Malcolm, 2009). More recently, the paradigm has shifted, and SOM degradation is viewed as a result of a variety of controlling factors, both intrinsic, like carbon to nitrogen ratio, and extrinsic, like microbial community composition and soil stabilization (Schmidt et al., 2011). SOM can be stabilized through physical and chemical stabilization mechanisms (Six et al., 2002). Physical stabilization occurs when SOM forms aggregates with itself and with soil particles, physically blocking the molecules on the inside of the aggregate from microbial decomposers and enzymes (Elliott and Coleman, 1988). Chemical stabilization occurs when SOM bonds or sorbs to silt and clay particles in the soil (Hassink, 1997). Aggregation, in combination with other environmental factors, can significantly affect the rate at which SOM degrades.

1.3 Mycorrhizal fungi

Mycorrhizal fungi associate with the roots of plants in a symbiotic relationship (Lakhanpal, 2000). In the late 1800s, Albert Bernhard Frank coined the term "mycorrhiza", which means "fungus-root" (Frank, 1894), and noted that mycorrhizal fungi play a role in the decomposition of litter and the nutrition of trees (Tunlid and Lindahl, 2015). Although Frank published his "mycorrhizal decomposition theory" in 1894, mycorrhizal fungi have for the most part been overlooked as part of SOM decomposition until recently.

Ectomycorrhizal (ECM) fungi are mycorrhiza that live on the outside of plant roots and comprise up to 50% of microbial biomass in forest soils (Bååth et al., 2004). ECM fungi live in symbiosis with the tree they associate with in which the tree allocates carbon

to the fungus and the fungus gathers nutrients, such as nitrogen, for the tree (Figure 1.1). ECM fungi break down the organic molecules in which nitrogen is embedded in the soil, including amino acids, amino sugars, proteins and peptides, and heterocyclic molecules, to make nitrogen accessible to plants (Shah et al., 2016).

ECM fungi obtain metabolic carbon from their tree symbiont and are therefore biotrophs (Baskaran et al., 2017). Trees allocate up to 40% of their net primary production to the ECM fungi on their roots (Baskaran et al., 2017; Hobbie, 2006). The magnitude of carbon allocation is dependent on external factors, namely nutrient availability in the soil. It is also affected by anthropogenic changes to the environment, such as increased carbon dioxide in the atmosphere and nitrogen deposition (Hobbie, 2006). For example, under elevated carbon dioxide conditions, plant growth increases and more ECM fungi grow on the roots, accepting more carbon from the plant (Norby et al., 1986; Rillig et al., 2002).

The relationship between trees and ectomycorrhizal fungi falls on a mutualism-parasitism spectrum (Baskaran et al., 2017). Mutualism occurs when both the fungus and the tree benefit, while in a parasitic relationship, the fungus benefits while the tree suffers (Johnson et al., 1997). Whether the fungi are beneficial or parasitic to the tree depends on the cost to benefit ratio between the amount of carbon allocated to the fungus and the amount of nitrogen returned to the tree. When nitrogen is limited in the soil, trees are unable to accumulate sufficient nitrogen on their own and rely more on ECM fungi, shifting the relationship toward mutualism. For that reason, ectomycorrhizal fungi play a more important role in the decomposition of SOM under nitrogen-limited conditions. Under such conditions, the fungi are responsible for mining more nitrogen for the tree, thereby decomposing more SOM and decreasing carbon storage (Baskaran et al., 2017). The

relative importance of ECM fungi to carbon cycling is affected by these environmental factors.

1.4 Fungal cell wall chemistry

Polysaccharides, proteins, and melanin form the cell walls of ectomycorrhizal fungi (Figure 1.2). The main structural components of fungal cell walls are the polysaccharides chitin and glucan, and together they account for approximately 80% of cell wall mass (Bartnicki-Garcia, 1968). Chitin is a biopolymer composed of N-acetylglucosamine monomers. It forms fibrils that help hold the cell wall components together and acts as a "melanin anchor" (Nosanchuk et al., 2015). Glucans are polysaccharides composed of glucose monomers with α- or β-linkages. Proteins contribute approximately 15-30% of the mass of fungal cell walls (Smiderle et al., 2012). Proteins are made up of amino acid monomers connected by peptide bonds. Because of the prevalence of nitrogen in amino acids, proteins account for up to 70% of fungal cell wall nitrogen (Smiderle et al., 2012). Proteins exist in the cell membrane as well as the cell wall, where they are covalently bonded to the cell wall polysaccharides.

The term "melanin" refers to a group of pigments found across biological kingdoms, including fungi (Henson et al., 1999). Melanin is a secondary metabolite, meaning that it is not fundamental to growth but does increase survival (Butler and Day, 1998). It is found in the cell walls of fungi, providing both structure and protection. Melanin can protect fungi from ultraviolet radiation by blocking over 90% of this radiation (Feofilova, 2010) and dispersing the energy from light as heat (Butler and Day, 1998). The unpaired electrons in melanin allow it to act as an antioxidant and therefore protect fungal

cells from oxidizing agents in the soil (Feofilova, 2010). Melanin can also protect fungi from water stress, as shown in *Cenococcum geophilum* (Fernandez and Koide, 2013). It has been shown that high-melanin fungi become dormant when water is limited and are revived when water becomes abundant. On the contrary, low-melanin fungi do not tend to survive drought conditions (Butler and Day, 1998).

The structure of melanin is largely unknown. It differs between species and is often complexed with other cell wall components, further complicating its elucidation (Butler and Day, 1998). Known information about melanin's structure includes that it is a biopolymer with a complex, irregular structure of phenolic and indolic monomers, making it highly aromatic (Bull, 1970). Solid-state nuclear magnetic resonance (NMR) of melanin found evidence of aliphatic carbons bonded to oxygen, aromatic and olefinic carbons, carbonyls, and methylene groups (Tian et al., 2003). Melanin is unhydrolyzable and insoluble in acid, and oxidative enzymes are required to break it down (Fernandez and Koide, 2014).

Some classes of melanin have been identified by monomers present in the polymer, but the precise structure, especially how the monomers are linked, is still unclear. L-dihydroxyphenylalanine (L-DOPA, Figure 1.3a) is the monomer of the type of melanin produced by humans, but is found in some fungi as well (Butler and Day, 1998). Pheomelanin, which has a reddish-brown color and is composed of benzothiazine monomers (Figure 1.3b), is derived from L-DOPA, but incorporates sulfur into the structure (Wakamatsu and Ito, 2002). Due to the sulfur atom within the structure of the benzothiazine monomer, the amount of sulfur in pheomelanin is high, ranging from 9 to 12% (Ito and Fujita, 1984). Eumelanin, a third type of melanin, is dark brown or black in

color and composed of dihydroxyindole monomers (Figure 1.3c) (Wakamatsu and Ito, 2002). It contains 6-9% nitrogen and up to 1% sulfur. Glutaminyl-4-hydroxybenzene (GHB) (Figure 1.3d) and glutaminyl-3,4-dihydroxybenzene (GDHB) are monomers of melanin in some fungi (Butler and Day, 1998). Lastly, the most studied class of fungal melanin is allomelanin. The term "allomelanin" encompasses dark pigments composed of monomers without nitrogen (d'Ischia et al., 2013). It is important to note that although allomelanin does not contain nitrogen, it may appear to contain nitrogen when analyzed chemically because the linkages between monomers could contain nitrogen and because melanin is often associated with proteins which do contain nitrogen (Butler and Day, 1998). A common and well-studied allomelanin monomer is dihydroxynaphthalene (DHN) (Figure 1.3e), found in melanin produced by Ascomycetous fungi such as *Cenococcum geophilum* (Fernandez and Koide, 2013).

There is evidence that melanin is found covalently bonded to other cell wall components, namely polysaccharides and aliphatic compounds, in order to hold the melanin in place (Bull, 1970). Some ECM fungal species, such as *Meliniomyces bicolor*, incorporate more aliphatic compounds into the melanin structure during melanogenesis in order to bind melanin to the cell wall (Zhong et al., 2008). These species-level changes to the chemical composition of the melanin further complicate the characterization of its structure(s).

Melanin content affects the rate of necromass degradation. In studies of high- and low-melanin versions of the same species of fungus, the low-melanin necromass lost significantly more mass at each harvest than the high-melanin necromass (Fernandez and Kennedy, 2018; Fernandez and Koide, 2014). If the only difference between high- and low-

melanin types of a species is the melanin content, and if the high-melanin necromass degrades at a significantly slower rate, it can be implied that melanin is a factor controlling the rate at which ECM fungal necromass degrades. Melanin also has inhibitory effects on the extracellular enzymes that are responsible for breaking down cell wall components – chitinase, glucanase, and protease – causing chitin, glucan, and proteins, respectively, to degrade more slowly in its presence (Kuo and Alexander, 1967). Chitinase activity, in particular, can be halted entirely in the presence of melanin (Bull, 1970). In addition to enzyme inhibition, melanin can bind to chitin, forming a melanin-chitin complex. Chitin bound to melanin in these complexes is less degradable than unbound chitin (Bull, 1970).

Other cell wall components degrade at different rates. Generally, proteins are degraded quickly because they are susceptible to hydrolysis and because they contain nitrogen, a desirable nutrient (Kögel-Knabner, 2002). Glucans also degrade relatively quickly (Drigo el al., 2012). Discrepancies exist about how quickly chitin is degraded. Traditionally, chitin has been thought to be relatively resistant to decomposition (Swift et al., 1979). More recent studies, however, have shown that the concentration of chitin in fungal necromass decreases rapidly at the beginning of degradation, implying it is easily degraded (Fernandez & Koide, 2012; Schreiner et al., 2014). Glucan and chitin can bind to melanin, though; these polysaccharide-melanin complexes are more resistant to degradation than the polysaccharides alone (Bull, 1970).

1.5 Summary and statement of the problem

ECM fungi play an especially relevant role in the carbon cycle because they obtain carbon from the atmosphere through their symbionts and direct that carbon belowground,

where it has the potential to be stored long-term. ECM fungal necromass in the soil can contribute to long-term SOM storage if it is stable. On the contrary, if the necromass is degraded completely and broken down to carbon dioxide or methane, it can be released from the soil, acting to return greenhouse gases to the atmosphere.

Thus, identifying which factors control which degradation pathway ECM fungal necromass takes is important to understanding the dynamics of the carbon cycle. Additionally, analyzing how the bulk chemistry of fungal necromass changes as it degrades over time provides insight into the decomposition of cellular components. This research aims to show that dynamic chemical changes occur as ECM fungal necromass degrades, especially during the first week of degradation. This initial degradation period has been overlooked in other degradation studies but contains important information about the degradation of cell wall components. These changes can be analyzed semi-quantitatively by employing novel techniques in thermochemolysis-gas chromatography-mass spectrometry. Understanding the bulk chemistry of fungal necromass and how it changes over time aids in understanding how necromass degrades on a molecular level.

Chapter 2 of this thesis details the methods and results of a field degradation study performed to gain insight into the chemical changes that occur as ECM fungal necromass degrades and what factors control the rate of its degradation. It is formatted to be submitted for publication in the Soil Biology & Biochemistry journal, and therefore some of the background information covered in the introduction will overlap with that covered in this literature review. Chapter 3 presents supplementary information, detailed protocols, and additional data gathered but not included in the paper submitted for publication.

CHAPTER 2

2.1 Introduction

Twice as much carbon is stored in soil organic matter (SOM) as exists as carbon dioxide in the atmosphere, totaling an estimated 1500 Pg in the top meter of soil globally (Jobbágy & Jackson, 2000). Traditionally, aboveground litterfall from plants, such as leaves and needles, was thought to contribute the majority of organic matter to long-lived SOM (Swift, 1979). However, evidence gathered in recent years suggests that belowground inputs, such as plant roots and soil microbes, contribute more carbon to SOM than previously estimated. In fact, it was shown that up to 70% of the carbon in forest soils originates from belowground sources (Clemmensen et al., 2013). As major contributors to long-lived SOM, belowground inputs are important to the global carbon cycle.

Soil has the potential to act as a source or a sink of carbon. When SOM degrades, it can be broken down to carbon dioxide or methane and respired into the atmosphere. If the amount of carbon dioxide respired exceeds the input of carbon into soil, soil becomes a net carbon source. On the contrary, if that SOM is stable, it can remain belowground long-term, effectively sequestering carbon out of the atmosphere. The degradation of SOM is affected by a variety of factors, including intrinsic chemical quality and soil stabilization. Traditionally, the rate of SOM degradation has been thought to depend solely on the biochemical "quality" of the organic matter, especially the ratio of carbon to nitrogen in the SOM (Swift, 1979). Organic matter high in nitrogen tends to be degraded more quickly than organic matter low in nitrogen because nitrogen is a valuable nutrient and therefore desirable to decomposers. This trend was demonstrated in birch leaf litter (Cotrufo et al., 1995), litter from conifers and hardwoods (Melillo et al., 1982; Taylor et al., 1989), and

fungal necromass (Fernandez & Koide, 2014; Koide & Malcolm, 2009). More recently, the paradigm has shifted, and SOM degradation is viewed as a result of a variety of controlling factors, both intrinsic, like carbon to nitrogen ratio, and extrinsic, like microbial community composition and soil stabilization (Schmidt et al., 2011). SOM can be stabilized by soil both physically and chemically (Six et al., 2002). Physical stabilization occurs when SOM forms aggregates with itself and with soil particles. The molecules on the inside of the aggregate are physically protected from microbial decomposers and enzymes by the outer layers of the aggregate (Elliott and Coleman, 1988). Alternatively, SOM can chemically associate to silt and clay particles in the soil, which provides chemical protection (Hassink, 1997). This, in combination with other factors, affects the rate at which SOM degrades.

The turnover of soil fungus has gained recognition as a major input of carbon into soil, contributing to the long-term accumulation of SOM (Godbold et al., 2006; Kögel-Knabner, 2002). Mycorrhizal fungi have been shown to contribute more than half of the total carbon found in SOM, totaling more than leaf litter and fine root turnover combined (Godbold et al., 2006). Mycorrhizal fungi associate with the roots of plants in a symbiotic relationship (Lakhanpal, 2000). In the late 1800s, Albert Bernhard Frank coined the term "mycorrhiza", meaning "fungus-root" (Frank, 1894), and noted that mycorrhizal fungi play a role in the decomposition of litter and the nutrition of trees (Tunlid and Lindahl, 2015). It has been demonstrated that degradation-resistant SOM looks more like microbial products than plant products on a molecular level, reinforcing the theory that soil microbes play an important role in the soil carbon cycle (Kallenbach et al., 2016; Simpson et al., 2007). The chemical similarities between microbial-derived organic matter and SOM, in

addition to the demonstrated retention of microbial-derived organic matter in soils, suggest that fungi may play a more important role in soil carbon storage than previously assumed.

Ectomycorrhizal (ECM) fungi, a subset of mycorrhizal fungi, live on the outside of tree roots. ECM fungi are widespread in forests, comprising up to 50% of microbial biomass in forest soil (Bååth et al., 2004; Högberg and Högberg, 2002). ECM fungi are biotrophs: they obtain metabolic carbon from their tree symbiont (Baskaran et al., 2017) (Figure 2.1). In exchange for that carbon, ECM fungi break down nitrogen-containing organic matter in the soil and return nitrogen to the tree (Shah et al., 2016). Trees allocate up to 40% of their net primary production to the ECM fungi associated on their roots (Baskaran et al., 2017; Hobbie, 2006). The magnitude of carbon allocation is dependent on external factors, namely nutrient availability in the soil, and is affected by anthropogenic changes to the environment, such as increased atmospheric carbon dioxide and nitrogen deposition (Hobbie, 2006). Elevated carbon dioxide conditions induce photosynthesis, providing plants with more carbon to allocate belowground to their ectomycorrhizal symbionts (Norby et al., 1986; Rillig et al., 2002). Under elevated soil nitrogen conditions, nitrogen is more readily available to trees and therefore trees rely less on ECM fungi to harvest nitrogen for them, so carbon allocation to ECM fungi decreases (Baskaran et al., 2017). The effects of the changing climate on soil carbon storage are complex and currently being investigated.

Fungal cell walls are composed of polysaccharides, proteins, and melanin (Figure 2.2). The main structural components of fungal cell walls are the polysaccharides chitin and glucan, and together they account for approximately 80% of cell wall mass (Bartnicki-Garcia, 1968). Chitin is a biopolymer composed of N-acetylglucosamine monomers. It

forms fibrils that help hold the cell wall components together and acts as a "melanin anchor" (Nosanchuk et al., 2015). Glucans are polysaccharides composed of glucose monomers with α- or β-linkages. Proteins contribute approximately 15-30% of the mass of fungal cell walls (Smiderle et al., 2012). Proteins are made up of amino acid monomers connected by peptide bonds. Because of the prevalence of nitrogen in amino acids, proteins account for up to 70% of fungal cell wall nitrogen (Smiderle et al., 2012). Proteins exist in the cell membrane as well as the cell wall, where they are covalently bonded to the cell wall polysaccharides.

Fungal cell walls also contain melanin, although how much varies between species (Butler and Day, 1998). The term "melanin" refers to a group of pigments found across biological kingdoms, including fungi (Henson et al., 1999). The structure of melanin is largely unknown. It differs between species and is often complexed with other cell wall components, further complicating its elucidation (Butler and Day, 1998). Known information about melanin's structure includes that it is a biopolymer with a complex, irregular structure of phenolic and indolic monomers, making it highly aromatic (Bull, 1970) (Figure 2.3). The biopolymeric nature of melanin differentiates it from other pigments, like carotenoids and chlorophyll, which are discrete molecules. Melanin is a secondary metabolite, meaning that it is not fundamental to growth but does increase survival by providing protection from ultraviolet light, drought, and oxidizing agents in the soil (Butler and Day, 1998; Feofilova, 2010; Fernandez and Koide, 2013).

In addition to its protective capabilities, melanin has been shown to decrease the rate of degradation of ECM fungal necromass (Fernandez and Kennedy, 2018; Fernandez and Koide, 2014). In studies of high- and low-melanin versions of the same species of

fungus, the low-melanin necromass lost significantly more mass at each harvest than the high-melanin necromass (Fernandez and Kennedy, 2018; Fernandez and Koide, 2014). Melanin itself is resistant to degradation (Butler and Day, 1998). In addition, melanin has inhibitory effects on the extracellular enzymes that are responsible for breaking down cell wall components – chitinase, glucanase, and protease – causing chitin, glucan, and proteins, respectively, to degrade more slowly in its presence (Kuo and Alexander, 1967). Chitinase activity, in particular, can be halted entirely in the presence of melanin (Bull, 1970). In addition to enzyme inhibition, melanin can bind to chitin, forming a melanin-chitin complex. Chitin bound to melanin in these complexes is less degradable than unbound chitin (Bull, 1970).

Other cell wall components degrade at different rates. Generally, proteins are degraded quickly because they are susceptible to hydrolysis and because they contain nitrogen, a desirable nutrient (Kögel-Knabner, 2002). Glucans also degrade relatively quickly (Drigo el al., 2012). Discrepancies exist about how quickly chitin is degraded. Traditionally, chitin has been thought to be relatively resistant to degradation (Swift et al., 1979). More recent studies, however, have shown that the concentration of chitin in fungal necromass decreases rapidly at the beginning of degradation, implying it is easily degraded (Fernandez & Koide, 2012; Schreiner et al., 2014) . Glucan and chitin can bind to melanin, though, and these polysaccharide-melanin complexes are more resistant to degradation than the polysaccharides alone (Bull, 1970).

Understanding the degradation of belowground inputs of carbon is important to understanding the contributions of soil to the global carbon cycle. ECM fungi are especially relevant because they remove carbon dioxide from the atmosphere on a large scale in

forests. How ECM fungal necromass degrades determines whether that carbon remains belowground long-term and is effectively sequestered or whether it is respired back into the atmosphere, becoming a source of greenhouse gases. Retaining carbon below ground allows ECM fungi to act as a carbon sink and not a source, limiting the amount of carbon dioxide respired back into the atmosphere.

For that reason, identifying which factors control which degradation path ECM fungal necromass takes is important to understanding the dynamics of the carbon cycle. Additionally, analyzing how the bulk chemistry of fungal necromass changes as it degrades over time provides insight into the decomposition of cellular components. This research aims to show that dynamic chemical changes occur as ECM fungal necromass degrades, especially during the first week of degradation. This initial degradation period has been overlooked in other degradation studies but contains important information about the degradation of cell wall components. These changes are analyzed semi-quantitatively by employing novel techniques in thermochemolysis-gas chromatography-mass spectrometry. Understanding the bulk chemistry of degrading fungal tissue and how it changes over time aids in understanding how necromass degrades on a molecular level.

2.2 Methods

2.2.1 Necromass generation

Necromass of four ectomycorrhizal species was generated (Figure 2.4): *Cenococcum geophilum* (CG) and *Meliniomyces bicolor* – black (MBb) (high-melanin), and *Suillus punctipes* (SP) and *Meliniomyces bicolor* – white (MBw) (low-melanin). Isolates of each species were grown in 50 mL half-strength potato dextrose broth (100 mL

for *Meliniomyces bicolor* – white) in 125 mL flasks. Flasks were shaken at 80 RPM at room temperature on orbital shakers for 30 days. Fungal colonies were harvested, rinsed with deionized water and oven-dried for 24 hours at 27 °C. The resulting necromass (21 mg – 120 mg) was placed in nylon mesh litter bags (3 × 3 cm, 53 µm mesh), heat-sealed, and each bag was attached to a metal numbered tag for later identification.

2.2.2 Field degradation

Bags were buried below the soil litter layer in a *Pinus*-dominated forest at Cedar Creek Ecosystem Science Reserve (45°25'16" N, 93°11'49" W) on June 27th, 2018. Additional site information is provided in Section 3.1. Bags were buried under the soil litter layer, 10 cm apart in each of four plots, and allowed to degrade naturally. Each plot was 10 m apart to account for soil and environment heterogeneity. Four replicates of each species on each day (1 per plot) were harvested after 0, 1, 2, 4, 7, 14, 28, 60, and 90 days. Day 0 bags were harvested after spending approximately 1 hour in the soil (immediately after burial) and are considered "control" undegraded samples in this study. Focusing on the first week of incubation for bag harvest allowed us to look more closely at the dynamic early degradation period of the fungal necromass.

2.2.3 Sample processing

At harvest, bags were removed from the soil, placed in individual pre-combusted, carbon-free glass jars, and transported on ice back to the lab (a trip of approximately 3 hours). Immediately upon arrival to the laboratory, necromass was removed from mesh bags, placed in pre-weighed, pre-combusted 20 mL glass scintillation vials, and frozen

overnight. Necromass was then freeze-dried, weighed, and ground to fine powder with a Wig-L-Bug grinding mill. For harvest days 0 through 14, mass loss was determined from pre- and post-incubation dry weights. Samples were stored in glass scintillation vials in a desiccator.

At some point between harvest days 14 and 28, some of the bags were removed from the soil, presumably by an animal (Section 3.1). By day 60, most of the bags had been removed from the soil and were not located near tags. Because of this, it is impossible to know with certainty the initial masses of these bags to accurately calculate mass loss. Therefore, mass loss for harvest days 28, 60, and 90 was calculated by averaging the initial masses of the bags remaining of each species and averaging the final masses of bags collected. These data are presented with open circles in mass loss figures.

2.2.4 Elemental analysis

Elemental analysis (EA) was run on a Costech elemental analyzer. Samples were weighed in tin capsules. A set of standards was run every 10 samples. Standards used were acetanilide (71.09% C, 10.36% N), caffeine (49.48% C, 28.85% N), natural-abundance sorghum (41.58% C), and low-organic content soil (1.61% C, 0.13% N). Standard error was less than 0.6% for %C and 0.4% for %N.

2.2.5 Thermochemolysis-Gas Chromatography-Mass Spectrometry

Necromass was analyzed by thermochemolysis-GCMS (pyGCMS) (Coban-Yildiz et al., 2000; Section 3.2). Tetramethylammonium hydroxide (TMAH) was added to weighed, ground necromass as a methylating agent. Samples were heated to 300 °C at a

rate of 720 °C/min in a Gerstel Thermal Desorption Unit and immediately introduced into the GC column (HP-5MS, 30 m × 0.250mm, 0.25 µm film thickness). The GC-oven (Agilent Technologies, 7890B) was heated from 50 °C to 320 °C over 55 minutes and held at 320 °C for 10 minutes. Molecules were ionized in an Agilent Technologies 5977A mass spectrometer by electron ionization with a voltage of 70 eV.

Peaks were classified as aliphatics, aromatics, carbohydrates, nitrogen-containing, sterols, or compounds of unspecified origin by their mass spectra using ChemStation software and the NIST library (Section 3.3; Table 3.1). Fatty acids and fatty alcohols were included in the aliphatic category. N-containing included proteins and amino sugars; N-containing chitin compounds were included in the N-containing category, not carbohydrates. Single ion monitoring (SIM) was performed by MassHunter (Table 3.2). Relative abundance of each classification of compound was calculated using a MATLAB script (Section 3.4).

2.2.6 Fourier Transform Infrared Spectroscopy

Ground necromass was analyzed with attenuated total reflectance-Fourier transform infrared spectroscopy (ATR-FTIR) (Thermo Scientific, Nicolet iS10). Wavenumbers ranged from 40 to 4000 cm^{-1} with a resolution of 4.0 cm^{-1} for 100 scans. Peak areas were deconvoluted and quantified using PeakFit software.

2.2.7 Melanin isolation

Melanin was isolated from ground necromass based on a method from Prados-Rosales (2015) (Section 3.5). Briefly, approximately 0.5 g freeze-dried necromass was

suspended in a solution of phosphate-buffered saline (PBS), buffer (1 M sodium citrate, 0.1 M sorbitol, pH 5.5), and lysing enzyme (10 mg/mL) and incubated at 30 °C for 24 hours. The sample was centrifuged to collect the pellet and washed five times with PBS. A 4 M solution of guanidine thiocyanate was added and the sample was incubated at room temperature overnight with constant shaking. After centrifugation and PBS wash, buffer (10 mM TrisHCl, 5 mM calcium chloride, 5% SDS, pH 8.0) and proteinase K (1 mg/mL) were added and it was incubated at 65 °C for 4 hours. The sample was centrifuged and the pellet was resuspended in PBS. A solution of methanol and chloroform (2:1 by volume) was added to achieve a final ratio of 4:2:1 chloroform:methanol:aqueous. The chloroform layer was isolated and disposed of. The remaining mixture was acid hydrolyzed with 6 M hydrochloric acid and heated for 1 hour. The hydrolyzed product was dialyzed (MWCO 12 kDa) against MilliQ water for 72 hours at 4 °C with constant stirring and daily water changes. The remaining mixture was freeze-dried to collect the melanin. Melanin content is presented as milligrams of melanin per grams of bulk tissue.

2.2.8 Kinetic modeling and statistical analysis

Rate constants were determined for exponential, Single-G, and Multi-G (biexponential) models (Section 3.6). Exponential rate constants k_{exp} were calculated by dividing the natural log of the relative mass remaining after 90 days of degradation by 90 days. (Fernandez and Koide, 2014). For the Single-G model, the natural log of the relative mass remaining at each harvest day was plotted versus time (Berner, 1964). The rate constant was the negative slope, determined by linear regression with the y-intercept set to 0, and is reported as k_{sg} in Table 2.3.

Degradation of each species was fit with a Multi-G model with two pools of carbon: one fast-degrading and one slow-degrading (Westrich and Berner, 1984). The model was fit by alternating adjusting the rate constants, k_1 and k_2, and relative amounts of each pool, β_1 and β_2, to minimize the sum of the squared residuals (SSR). The fit was adjusted a total of eight times, at which point the decrease in SSR between iterations was less than 0.001.

Statistical significance was determined using single-factor ANOVA with an alpha of 0.05. Calculated p-values are reported.

2.3 Results

2.3.1 Extent of degradation

Necromass of the four ECM species degraded over the course of 90 days (Figures 2.5-2.8). Mass loss was rapid at the beginning of incubation and slowed as time progressed. Three species lost more than half the initial mass in the first seven days of incubation: CG lost 74%, SP lost 69%, and MBw lost 64%, on average. After approximately one month of degradation, the mass loss of each species stabilized. After 90 days, a fraction of each species remained; none of the samples were completely degraded.

CG, SP, and MBw degraded at essentially the same rate while MBb had lost significantly less mass at each harvest ($p < 0.05$). MBb lost only 28% of its mass after 7 days and 68% after 90 days (Figure 2.6). Although the rate of degradation differed from the other three species, it followed a similar pattern: faster decomposition during the first week and a plateau after one month.

2.3.2. Initial nitrogen and melanin content

The C/N ratio of undegraded MBb was significantly higher than the other three species at 18.6 ± 3.8 ($p < 0.05$) (Figure 2.9). Unsurprisingly, MBb also contained significantly less nitrogen than the other species with 2.81% ($p < 0.05$) (Figure 2.10).

Melanin content from melanin isolation ranged from 7 to 160 mg melanin g^{-1} bulk necromass (Table 2.1). MBb contained the most melanin at 160 mg melanin g^{-1} bulk necromass. SP, despite being visually darker than MBw (Figure 2.4), contained the least amount of melanin at 7 mg melanin g^{-1} bulk necromass. The fungal melanin content presented here is lower than the melanin content reported for some of the same species in previous studies (Fernandez and Kennedy, 2018; Fernandez and Koide, 2014; Table 2.1). In this study, melanin was biochemically isolated from dried necromass (Prados-Rosales et al., 2015). Melanin content was calculated by dividing the dry mass of melanin isolated by the dry mass of bulk necromass from which it was isolated. Other studies have used an Azure A colorimetric assay to estimate melanin content (Fernandez and Kennedy, 2018; Fernandez and Koide, 2014). The isolation method resulted in lower melanin content across species than the assay (Table 2.1).

2.3.3. Chemical changes during degradation

The significant mass loss in the first week of incubation was accompanied by changes in the chemical composition of the necromass. Aliphatic compounds and

carbohydrates made up most of the mass of necromass of all four species (Figures 2.5-2.8). This remained true throughout the degradation sequence.

In CG necromass, the carbohydrate content decreased after two days, causing a brief increase in aliphatic content (Figure 2.5). Then, aliphatic content decreased and relative carbohydrate content increased over the remainder of the sequence. Sterol content, while steady for the first week, increased thereafter.

MBb necromass contained significantly more aliphatic compounds than the other species before incubation and throughout the degradation sequence ($p < 0.05$) (Figure 2.6). As incubation progressed, the relative abundances of the different classifications of compounds remained relatively constant until the day 28 harvest, at which point aliphatic content decreased and carbohydrate content increased.

The relative abundance of the different components in SP necromass remained relatively constant for the first week of degradation (Figure 2.7). After seven days, the aliphatic content decreased and the relative abundance of carbohydrates increased. Sterol content of SP necromass increased after 60 and 90 days, peaking at day 60.

During the first four days of incubation, carbohydrate content of MBw necromass decreased (Figure 2.8). At the same time, there was an increase in the relative abundance of aliphatic compounds. After four days, aliphatic content sharply decreased and carbohydrate content increased.

Degraded necromass is chemically distinct from fresh necromass (Figure 2.11). Across all four species, degraded necromass contains a lower relative abundance of aliphatic compounds than fresh necromass. This decrease in aliphatics is accounted for with a higher

relative abundance of carbohydrates and sterols at the end of the degradation sequence. Additionally, the relative abundance of aromatic compounds is higher at the end of the degradation study than at the beginning for each of the four species (Figure 2.12).

FTIR spectra from CG and SP also demonstrate that degraded necromass is distinct from undegraded necromass (Figure 2.13). Five peaks were identified in the carbohydrate region of CG and SP necromass, from 1180 to 830 cm^{-1} (Table 2.2). In this region, peaks broadened from day 0 to day 90 (Figure 2.13). From the day 0 spectrum it is evident that the carbohydrate region contains five peaks (Figure 2.13a,c). At day 90, though, this region appears as one large peak and a small peak on either end for both CG and SP necromass (Figure 2.13b,d).

2.4 Discussion

2.4.1 Extent of degradation

Mass loss of each of the four species was fit to an exponential fit, a Single-G model, and Multi-G model (Table 2.3, Figure 2.14, Section 3.6). The Single-G model presents the degradation of organic matter as a first-order reaction in which the organic matter decays exponentially (Berner, 1964). The Single-G model presumes:

$$G_t = G_0 e^{-kt} \tag{2.1}$$

where G_0 is the initial mass of organic matter, k is the first-order rate constant, and G_t is the mass of organic matter remaining at time t. These rate constants are reported in Table 2.3 as k_{sg}. In order to make direct comparisons to the literature, exponential rate constants

were also calculated by dividing the negative natural log of relative mass remaining at day 90 by 90 days (Fernandez and Koide, 2014). These differ slightly from those calculated by modeling the entire degradation as in the Single-G model and are reported in Table 2.3 as k_{exp}.

The degradation of fungal necromass was better represented by the Multi-G model (Figure 2.14). The Multi-G model posits that there are two pools of organic carbon degrading simultaneously, following Equation 2.2:

$$G_t = G_1 e^{-k_1 t} + G_2 e^{-k_2 t} \quad (2.2)$$

where G_1 and G_2 are the mass of organic matter in the fast- and slow-degrading pools, respectively, and add up to G_0 (Westrich and Berner, 1984). G_1 and G_2 decay exponentially according to rate constants k_1 and k_2 where $k_1 > k_2$ (Table 2.3). Initially, the degradation of G_1 with rate constant k_1 dominates the overall degradation rate and degradation is rapid. After the majority of that pool has degraded, the overall degradation rate slows as it becomes dominated by the degradation of G_2 with slower rate constant k_2. This is a better fit than the Single-G model because the observed degradation is rapid initially and slows down as degradation proceeds (Table 3.3).

Melanin is a major contributor to, and controls the rate of degradation of, the slow-degrading pool. Rate constant k_2 is negatively correlated to melanin content ($R^2 = 0.92$, $p < 0.05$; Figure 2.15a). There is no correlation between melanin content and k_1 ($R^2 = 0.007$, $p > 0.70$; Figure 2.15b). As melanin content increases, the slow-degrading portion of fungal necromass degrades more slowly. This supports the theory that melanin itself degrades

more slowly than other cellular components and that it slows the overall degradation of fungal necromass (Fernandez & Kennedy, 2018; Fernandez & Koide, 2014).

Fungal necromass in this study degraded quickly relative to other forms of organic matter whose degradation has been studied (Table 2.3). Rate constants for fungal degradation were one to two orders of magnitude greater than rate constants for the degradation of leaves from various species of trees (Fioretto et al., 2005; Hasanuzzaman & Hossain, 2014; Melillo et al., 1982). However, it should be noted that the length of degradation study likely affects the rate constants reported. This degradation study lasted three months, whereas the leaf degradation studies used for comparison lasted six months to three years. Had this degradation study continued for a year or more, it is expected that little additional mass loss would occur. This would decrease k_2 as t increased but G_t/G_0 remained effectively constant. It is therefore possible that the rate constants from this study are artificially high in relation to those reported for longer degradation studies. To account for this, rate constants for the initial degradation period were estimated from published figures, as data tables were not available. In some cases, these values were larger than the reported rate constants that considered longer degradation times (Table 2.3). Even after recalculating these rate constants, the rate constants for the degradation of fungal necromass remained larger than those for the degradation of other types of organic matter. In cases where the organic matter degraded steadily across the degradation period or more rapidly toward the end, the estimated rate constant was not lower than the reported one. It is also possible that degradation in this study was accelerated by the litter bag technique, although this would not explain the enhanced acceleration of fungal necromass relative to plant matter because several of the leaf studies also employed this technique. The use of

litter bags can potentially speed up degradation in soils because organic matter can be chemically or physically stabilized by soil particles and aggregates (Bull, 1970; Fernandez et al., 2016; Hassink, 1997). Placing necromass in a mesh bag creates a barrier between the necromass and the soil which could limit the extent of protection and thereby accelerate mass loss (Karberg et al., 2008).

The rate of degradation of fungal necromass within a species is controlled by melanin content, but this does not necessarily hold true when compared between species. MBw lost more mass than MBb at each harvest day, in agreement with the data presented by Fernandez and Kennedy (2018). Rate constants k_{exp}, k_{sg}, and k_1 were two to four times larger for MBw than MBb, and k_2 was 14 times larger (Table 2.3). The primary difference between MBb and MBw necromass is melanin content. This suggests that, within a species of fungus, low-melanin necromass degrades more rapidly than high-melanin necromass. SP degraded at effectively the same rate as MBw, which further supports the hypothesis that low-melanin necromass degrades relatively quickly. CG, though, degraded faster than melanin content would have predicted. CG contains more melanin than MBw and SP, but less than MBb. If melanin content were the only factor controlling the rate of degradation, the mass loss of CG necromass would have fallen between MBb and the two low-melanin species. Instead, CG degraded at effectively the same rate as the low-melanin species (Figure 2.5).

Necromass from all four species degraded rapidly during the first week of degradation (Figure 2.14). It is common that other studies (*e.g.* Fernandez & Kennedy, 2018; Fernandez & Koide, 2012, 2014) wait until 14 or 28 days to harvest the first round of necromass and therefore the first week to month of degradation has not been thoroughly

studied. Rapid mass loss in the first week of more than half the initial mass has been documented in saprotrophic fungal necromass using similar experimental protocols to this study (Schreiner et al., 2014; Bruner, 2019). Despite differences in overall rates of mass loss mentioned above, soil organic carbon, total soil microbial biomass, and leaves similarly underwent more rapid mass loss in the first one to two months of degradation (Fernandez et al., 2019; Follett et al., 2007; Melillo et al., 1982). This suggests that there is a fast-degrading pool and slow-degrading pool of organic carbon degrading simultaneously and supports the use of the Multi-G model.

None of the species degraded completely by the end of the 90-day degradation period. The persistence of some amount of mass suggests that fungal necromass can contribute to long-term carbon storage belowground. The minimal mass loss that occurred from 28 days onward suggests that most mass loss happens within a month of burial; any remaining mass has the potential to be stored belowground long-term. This differs from previous ectomycorrhizal fungal necromass degradation studies, although those studies used 28 days as the first harvest (Fernandez and Kennedy, 2018; Fernandez and Koide, 2014), making direct comparisons difficult. The slight apparent increase in mass remaining of SP from day 28 to day 60 and of CG from day 60 to day 90 is potentially due to the growth of other microbes on the necromass or is an artifact of averaging the harvested and initial masses to account for site disturbance.

It has been demonstrated in previous studies of organic matter, and specifically fungal necromass, that an increase in organic matter nitrogen content increases the rate of organic matter degradation (Melillo et al., 1982; Fernandez & Koide, 2014). MBb contains significantly less nitrogen than the other three species, while CG contains the most (Figure

2.10). Although the relatively high melanin content of CG necromass would predict that it degrades slowly, the high nitrogen content would predict that it degrade rapidly. All four species lost more mass after 90 days of degradation than initial melanin or nitrogen content would predict, based on Fernandez & Koide (2014) (Figure 2.16). Fernandez & Koide also noted a correlation between the ratio of melanin content (mg melanin g^{-1} necromass) to nitrogen content (%N) and degradation rate constant, recognizing that both characteristics affect degradation rate (Fernandez and Koide, 2014). In terms of the ratio of melanin to nitrogen, though, each species degraded more slowly than the model predicted (Figure 2.17). This is because the predicted rate constants were larger than the observed rate constants, especially for SP and MBW (Figure 2.18). This most likely occurred because the melanin contents in this study, which were calculated by isolation, were lower than the melanin contents upon which the previous fit was based, which were determined using a colorimetric assay. The predicted rate constants for melanin content as low as in this study, then, were much higher than the observed rate constants.

CG necromass lost significantly more mass after one, two, and three months than CG necromass studied previously (Fernandez and Koide, 2014). Fernandez & Koide looked at wild-type CG necromass (212-248 mg melanin g^{-1} necromass by assay) and melanin-inhibited CG necromass. After three months, the wild-type CG necromass had lost approximately 40% mass, on average, whereas the melanin-inhibited CG necromass had lost just over 50% mass, on average. In this degradation study, CG necromass, containing 90 mg melanin g^{-1} necromass by isolation, lost nearly 60% mass in the first four days of degradation. Both studies used a litterbag technique to bury necromass so any acceleration of degradation in this study cannot be attributed to burial technique. It is possible, albeit

unlikely, that the melanin content of CG necromass in this study is even lower than the melanin-inhibited CG necromass from Fernandez and Koide's study, as the melanin content was not measured in melanin-inhibited necromass in that study. The melanin content in this study is approximately 40% that of the wild-type necromass Fernandez & Koide generated. If the melanin content in this study were indeed less than the melanin-inhibited necromass, it could account for the rapid degradation. It is most likely, though, that the high nitrogen content of CG, combined with the intermediate melanin content, caused it to degrade relatively rapidly.

2.4.2 Chemical changes in necromass during degradation

Degraded necromass is chemically distinct from undegraded necromass. The changes in relative abundance of the various classifications of compounds suggest that cellular components degrade at different rates. In-depth studies of the chemical changes that occur during degradation are uncommon and therefore there are only a handful of examples published in the literature. Similar chemical changes to those observed in this study, namely a decrease in aliphatic content, have been documented in mycorrhizal fungi (Certano et al., 2018), saprotrophic fungi (Schreiner et al., 2014; Bruner, 2019), plant matter (Wickings et al., 2012), and dairy manure (Calderón et al., 2006). This trend was documented in each of the four species in this study but is most noticeable in the degradation of MBb necromass (Figure 2.6). In saprotrophic fungi, there was little significant difference in lipid (aliphatic) and sugar (carbohydrates) between degraded and undegraded necromass for three of the four species studied (Bruner 2019). For the Ascomycota species, though, there was a decrease in relative lipid content as degradation

proceeded. Similarly, mycorrhizal necromass after a 12-week degradation period showed a decrease in relative absorbance of aliphatic FTIR peaks compared to undegraded necromass (Certano et al., 2018). In plant tissue, the lipid content of corn biomass decreased over a period of degradation in soil, as determined by pyGCMS (Wickings et al., 2012). Lastly, FTIR analysis of dairy manure degrading in soil revealed a decrease in fatty acid content, which would be assigned to the "aliphatic" pool in this study, as degradation proceeded (Calderón et al., 2006). Calderón et al. suggested that this phenomenon could be caused by decomposers utilizing fatty acids as a source of energy (2006).

There are conflicting reports about the rate of decomposition of cell wall polysaccharides, especially chitin (Drigo et al. , 2012; Fernandez & Koide, 2012; Swift et al., 1979). About half of the cell wall polysaccharides degraded during the first week of degradation for 3 of the 4 species studied (only 21% for MBb). This supports the studies that have determined that a portion of cell wall polysaccharides degrade quickly upon burial (Drigo et al., 2012; Fernandez & Koide, 2012). At the end of the degradation period, 5-25% of carbohydrates remained (for CG, SP, and MBw), suggesting that there is a portion of the carbohydrate pool that is resistant to degradation, as has been shown previously (Swift et al., 1979).

The relative abundances of aromatic compounds and sterols were higher in necromass that degraded for 90 days (60 days for MBw) than undegraded necromass across species (Figure 2.11). A relative increase in sterol content was also documented in four species of saprotrophic fungi over a 28-day degradation period (Bruner, 2019), and an increase in aromatic content was documented in mycorrhizal necromass degradation

(Certano et al., 2018). The increase in aromatic content demonstrates that aromatic compounds are more resistant to degradation than the other components, which has been demonstrated in melanin (Butler and Day, 1998) and lignin (Swift et al., 1979). The increase in sterol content, though, is likely due not to the recalcitrance of sterols but instead to growth of microbes on the necromass. Ergosterol, for example, is a fungi-specific sterol that has been shown to be labile in soil and is therefore a biomarker for living fungus, not degraded necromass (Nylund & Wallender, 1992). Increased sterol content, therefore, is evidence that soil microbes penetrated the pores in the mesh bags, attached themselves to the necromass, and were included in chemical analysis.

The increase in the relative abundance of aromatic compounds in degraded versus undegraded necromass across species can be attributed to melanin (Figure 2.12). Although the exact structure of melanin is unknown, it is known to be highly aromatic, as demonstrated by the monomers that have been identified (Figure 2.3) (Butler and Day, 1998; Wakamatsu and Ito, 2002). The aromatic compounds identified in necromass originate from melanin and therefore an increase in the relative abundance of aromatic compounds suggests an increase in the relative abundance of melanin. This is evidence that melanin itself is resistant to degradation.

Melanin content affects the magnitude of chemical changes as necromass degrades. After just seven days, MBw necromass is comparable to MBb necromass after 90 days, both in terms of chemical composition and mass loss (Figures 2.6, 2.8). The chemical changes that occurred as MBw necromass degraded are dynamic. Necromass from each harvest is chemically distinct from the previous harvest, even in the first week of degradation when harvest was frequent. On the contrary, the degradation of MBb

necromass is less dynamic; few changes in the relative abundances of the classes of compounds occur in the first week of MBb necromass degradation. Unlike in MBw necromass, there is no decrease in the relative abundance of carbohydrates in MBb necromass over the first four days of degradation. Minimal changes in the chemical composition of MBb necromass, especially in carbohydrate content, suggest that the melanin in MBb could be protecting the other cell wall components, especially carbohydrates, from degradation either physically, chemically, or biologically (Bull, 1970; Fernandez et al., 2016; Kuo & Alexander, 1967; Six et al., 2002). If the protection is physical, melanin acts as a barrier, shielding the rest of the cell wall from degradation (Bull, 1970). If the protection is chemical, melanin is bonded to the other components, making them more resistant to degradation (Fernandez et al., 2016). If the protection is biological, the presence of melanin inhibits the extracellular enzymes that break down cell wall polysaccharides (Kuo and Alexander, 1967). A combination of mechanisms is likely. Because MBw necromass contains less melanin than MBb necromass, the cell wall components of MBw necromass are not protected to the same extent, allowing for more rapid chemical changes.

In addition to changes in relative abundances, the structures of the biopolymers remaining in the necromass change, as demonstrated by FTIR spectra (Figure 2.13). The FTIR peaks in the carbohydrate region become broader on day 90 versus day 0. Peak broadening in the carbohydrate region was also documented in the degradation of saprotrophic fungi (Schreiner et al., 2014) and shrimp shells, which contain chitin (Stankiewicz et al., 1998). In general, peak broadening can be attributed to the biopolymers becoming more disordered as they degrade (Focher et al., 1992; Stankiewicz et al., 1998).

In this study, the peak broadening occurs as the peak at 1017 cm^{-1} shrinks. This decrease is associated with a decrease in the relative abundance of aliphatic ethers (Stankiewicz et al., 1998). Monomers of cell wall polysaccharides – chitin, glucan, and mannan – are linked with ether linkages (Feofilova, 2010). A decrease in the abundance of ethers demonstrates that these linkages are broken as degradation proceeds and the biopolymers are broken into smaller polymers and their monomers.

Melanin content affects the degradation of chitin, according to FTIR spectra. The peak at 1072 cm^{-1} is indicative of N-acetylglucosamine, the monomer of chitin (Pierce and Rast, 1995). In SP necromass, the area of this peak decreases with degradation time (Figure 2.19a; $R^2 = 0.73$, $p < 0.1$). An apparent decrease in this peak was also shown in the saprotrophic fungus *Fusarium avenaceum* (Schreiner et al., 2014). In CG necromass, there is no correlation between degradation time and this peak area (Figure 2.19b; $R^2 = 0.01$, $p > 0.8$). This suggests that chitin degrades more readily in SP necromass than in CG necromass. Melanin has been shown to slow the degradation of cell wall polysaccharides, especially chitin (Bull, 1970). The melanin in CG appears to protect chitin from degrading, while the melanin content of SP is sufficiently low to have little effect on chitin degradation.

2.4.3 The effects of global change

Climate change will alter the dynamics of soil fungus degradation and soil carbon storage. There is approximately twice as much carbon stored in soil as there is carbon dioxide in the atmosphere (Jobbágy & Jackson, 2000). If the dynamics of carbon exchange

between the soil and the atmosphere shift even slightly, large amounts of carbon dioxide could potentially be respired back into the atmosphere. Increased temperature and carbon dioxide can initiate a positive or negative feedback loop in terms of soil respiration. In a positive feedback loop, increased temperature leads to more rapid degradation of fungal necromass which causes more carbon dioxide to be respired into the atmosphere, thereby exacerbating climate change (Davidson and Janssens, 2006; Fernandez et al., 2019). In the case of a negative feedback loop, the amount of carbon respired into the atmosphere is outweighed by an increase in carbon allocated belowground (Davidson and Janssens, 2006). This occurs because elevated carbon dioxide levels may induce photosynthesis and suppress respiration (Drake et al., 1997) and therefore plants have more carbon to allocate belowground. Elevated temperature caused by increased carbon dioxide has complex effects on photosynthesis and respiration which could either increase or decrease soil carbon storage (Dusenge et al., 2018). If the amount of carbon allocated belowground exceeds the amount respired into the atmosphere, there would be a net increase in soil carbon storage (Davidson and Janssens, 2006).

In Minnesota, the average annual temperature and annual precipitation are rising (Moss, 2017). Elevated ambient temperature increases the rate of degradation of mycorrhizal fungal necromass (Fernandez et al., 2019). Similarly, soil respiration, attributed to decomposition of organic matter, increases with soil moisture during warmer periods (Wildung et al., 1975). This suggests that, as Minnesota's climate continues to change, soil organic matter will degrade more quickly. Unless the input of carbon exceeds the degradation and respiration, more rapid degradation will increase the flux of carbon dioxide from soil into the atmosphere.

MBb and other slowly-degrading species of ectomycorrhizal fungi may present as more powerful conduits for carbon sequestration belowground than fast-degrading fungi. After three months of degradation, there was more mass of MBb remaining than the other three species, suggesting that MBb may contribute more mass to the pool of long-lived SOM than the other three species. Slow-degrading species of ectomycorrhizal fungi, such as MBb, can store more carbon belowground than fast-degrading species. As the climate continues to change and degradation rates increase, the storage of carbon in high-melanin species of fungal necromass will be of great importance.

As the planet warms, the relative abundance of species of trees will shift as temperatures rise. Ectomycorrhizal community composition will shift in response. It was shown in northern Quebec that, as temperature increased, growth of *Larix laricina* (tamarack) increased while *Picea mariana* (black spruce) struggled to regenerate (Dufour-Tremblay et al., 2012). ECM fungi of the genus *Suillus* are prevalent on *Larix laricina* (Kennedy et al., 2018), while *Picea* is a host for *Meliniomyces bicolor* (Joint Genome Institute, 2019). Therefore, as temperature increases, it is expected that *Suillus* will become more abundant in northern regions while *Meliniomyces bicolor* will become less abundant. This shift will affect the dynamics of carbon storage. If low-melanin species, like *Suillus punctipes*, become more abundant while high-melanin species like *Meliniomyces bicolor* – black become less abundant, carbon could be cycled through the soil more rapidly. This shift has the potential to cause increased soil respiration, further elevating ambient carbon dioxide levels.

2.5 Conclusions

In general, fungal necromass degrades more rapidly than other forms of organic matter, including plant and microbial biomass. The degradation of fungal necromass is well represented as a biexponential decay function, where a portion of the necromass degrades rapidly and the other degrades more slowly. This was observed in the degradation of four species of ECM fungal necromass, as mass loss was rapid across the first week of the study and slowed drastically after one month. At the end of the 90-day study, mass of each species remained, implying that a portion of the necromass is resistant to degradation and could contribute to long-term carbon storage belowground. Within a species, melanin content affects degradation rate, as demonstrated by comparing MBb and MBw. Between species, though, nitrogen content affects degradation rate, as suggested by the rapid degradation of high-nitrogen CG compared to low-nitrogen MBb.

The chemical composition of degrading ECM fungal necromass is dynamic, and this study demonstrates the importance of frequent harvests during the rapidly-changing initial one to two weeks of necromass degradation. Shifts in the relative abundances of the six classifications of compounds occurred even at the beginning of the study when harvests were frequent. In general, these chemical changes mirror those of other types of organic matter. Approximately half of the carbohydrates degraded during the first week and broke into smaller units as they degraded, aliphatic compounds degraded steadily across the degradation period, and relative aromatic content increased toward the end of the study. The increase in the relative abundance of aromatic compounds suggests that melanin, which is highly aromatic, resisted degradation. In addition to being resistant to degradation itself, increased melanin content decreased the degradation of carbohydrates, namely

chitin. This suggests melanin was protecting cell wall polysaccharides. Determining how the bulk chemistry changes and how melanin affects those changes can enhance the understanding of the role of ECM fungi in the carbon cycle.

CHAPTER 3: SUPPLEMENTARY INFORMATION

3.1 Field site

The field degradation study was conducted in an old *Pinus*-dominated forest at Cedar Creek Ecosystem Science Reserve in East Bethel, MN (45°25'16" N, 93°11'49" W) (Figure 3.1). Bags were attached to a metal tag with an identification number to identify the species and initial mass of that sample. Nine bags of each species were buried in each of four plots. The bags were buried 10 cm apart, and the plots were approximately 10 m apart.

The site lies in the Anoka sand plain and therefore the soil is very sandy. Based on elemental analysis (EA), it is low in nitrogen (0.37% N, standard deviation = 0.14%). Organic carbon (OC) content was 4.07% on average (standard deviation = 1.72%). Thermochemolysis-gas chromatography-mass spectrometry (pyGCMS) of the soil shows it is high in aromatic compounds (~26%) (Figure 3.2).

3.2 Thermochemolysis-gas chromatography-mass spectrometry (pyGCMS)

Sample preparation

1. Weigh out approximately 70 ug of organic carbon *(~150 ug ground fungal necromass)* into a glass pyrolysis tube using a tared balance.
2. Use a methanol-rinsed syringe to dispense 15 uL of sonicated tetramethyl ammonium hydroxide (TMAH; 25% in methanol).
3. Gently place transport adapter into pyrolysis tube.
4. Load desired method (see below). Start run.
5. When prompted, unlock the thermal desorption unit (TDU). Remove pyrolysis tube from previous run and replace with pyrolysis tube with new sample. Lock the TDU (this will start the run).
6. Run a blank before each run.

Method

1. Sample in pyrolysis tube is heated to 300°C at a rate of 720°C/min using a Gerstel Thermal Desorption Unit and pyrolyzer.
2. Sample enters GC column (Agilent Technologies, HP-5MS, 30 m × 0.250 mm) where GC oven (Agilent Technologies, 7890B) temperature ramps from 50°C to 320°C over 55 minutes and is held at 320°C for 10 minutes.
3. Mass spectrometer (Agilent Technologies, 5977A) ionizes sample and detects fragments using a voltage of 70 eV with a three-minute solvent delay.

3.3 pyGCMS data analysis

1. Set threshold (1% area of largest peak) and label peaks with retention times.
2. Look at mass spectrum of each peak above threshold. Compare mass spectrum and retention time to library of previously categorized compounds.
3. Build a method in MassHunter with the retention time and characteristic m/z (may or may not be base peak) of each identified peak.
4. Analyze file using method. Manually click through each identified peak to ensure that the software picked the correct peak and the entire peak. Correct any errors.
5. Export table to Excel. Delete rows of peaks not identified.
6. Sort peaks alphabetically by classification (aliphatic, aromatic, carbohydrate, nitrogen-containing, sterol, unspecified).
7. Relative abundances of the six classification of compound (aliphatic, aromatic, carbohydrate, nitrogen-containing, sterol, and unspecified) can be determined using MATLAB or Excel.

<u>MATLAB</u>

1. In the column directly to the left of the retention times, assign a number to each classification (1 = aliphatic, 2 = aromatic, 3 = carbohydrate, 4 = nitrogen-containing, 5 = sterol, 6 = sterol).
2. Fill the two columns directly to the right of the peak areas with 0. Add a row of 0 at the bottom of the table, after the last retention time.

3. Open MATLAB software and open script. Type “Data=[]” to create a table to input data. Copy table from Excel, right click in the top left cell of the spreadsheet on MATLAB and click “Paste Excel Data”.
4. Run the script. If there is a single run to analyze, insert “%” into the script at the beginning of lines 25 through 27. When prompted “Input number of samps in Data matrix”, input “1” for one sample, “2” for two, etc. When prompted “Input value of weight used for samp”, input the weight of the sample in milligrams. When prompted “Input value of OC ratio used for samp”, input the %OC as a decimal or a percent.
5. The left column under “Avedataall” corresponds to the relative abundance of each classification of compound in the sample. The top value is the relative abundance of the classification labeled 1 (aliphatics), the second value is the relative abundance of the classification labeled 2 (aromatics), etc.

Excel

1. Sort the data alphabetically by classification, as described above.
2. Normalize the peak area to the sample mass times the %OC (Peak area / (Mass * %OC).
3. Calculate the sum of normalized peak areas.
4. Divide each normalized peak area by the sum of normalized peak areas to calculate contribution of each peak to total signal.
5. Sum the contribution from each classification to calculate the relative abundance of that classification.

3.4 MATLAB script

MATLAB script used to determine relative abundance of each classification of compound.

```
numofsamps=input('Input number of samps in Data matrix:
');
samplemeta=zeros(2, numofsamps);
sampvec=1:numofsamps;
for k=1:numofsamps
    fprintf('Sample %d \n', k)
    mg=input('  Input value of weight used for samp:
');
    rat=input('  Input value of OC ratio used for samp:
');
    samplemeta(1,k)=mg;
    samplemeta(2,k)=rat;
end
clear mg rat
samplemeta %check matrix of weights and ratios prior to
moving on
for k=1:numofsamps %calculate a column to normalize
data to OC
    for i=1:(length(Data)-1)
       Data(i,(4*k))=[Data(i,((4*k)-
1))]/[samplemeta(1,k)*samplemeta(2,k)];
    end
end
for k=1:numofsamps %percentage of total
    for i=1:(length(Data)-1)

Data(i,(1+(k*4)))=Data(i,(4*k))/(sum(Data(1:end,(4*k)))
);
    end
end
 %create a column on end for stdevs--Run when you the
for loop when you
 %have multiple samples
for i=1:(length(Data)-1)
      Data(i,end)=var([Data(i,[1+sampvec*4])]);
 end
Avedatad=zeros(6,numofsamps); %create matrix for day 1
data to save all ave values in (checks how large SIM
is)
```

```
for k=1:numofsamps %call to treat each day of data
columns
    iteration=1; %initialize an iterator value for the
while loop--keeps track of row in Data sheet
    for i=1:6 %call each of the different organic
categories 1-7 found in the first column
    sumcategory=0; %initialize the sum of the category
to zero for each entrance to the while loop
        while Data(iteration,1)==i
            if Data(iteration,(1+(k*4)))>= 0.01 %SIM
size threshold

sumcategory=Data(iteration,(1+(k*4)))+sumcategory;
            end
            iteration=1+iteration;
        end
    Avedatad(i,k)=sumcategory; %save completed sum to
the Avedataday1 matrix
    end
end
Avedataall=zeros(6,numofsamps+1); %create matrix for
day 1 data to save all ave values in
for k=1:numofsamps %call to treat each day of data
columns
    iteration=1; %initialize an iterator value for the
while loop--keeps track of row in Data sheet
    for i=1:6 %call each of the different organic
categories 1-6 found in the first column
    sumcategory=0; %initialize the sum of the category
to zero for each entrance to the while loop
        while Data(iteration,1)==i

sumcategory=Data(iteration,(1+(k*4)))+sumcategory;
            iteration=1+iteration;
        end
    Avedataall(i,k)=sumcategory; %save completed sum to
the Avedataday1 matrix
    end
end
Avedataall
Avedatad
clear Avedatad i k iteration  sumcategory
%bar(Avedataall', 'stack')
```

3.5 Fungal melanin isolation

Adapted from Prados-Rosales et al., 2015

Chemicals list: 1X phosphate-buffered saline, buffer A (1M sorbitol, 0.1M sodium citrate, pH 5.5), buffer B (10mM TrisHCl, 5mM calcium chloride, 5% sodium dodecyl sulfate), cell wall lysing enzyme from *Trichoderma harzianum* (Sigma L1412), guanidine thiocyanate, proteinase K, chloroform, methanol, hydrochloric acid, dialysis tubing (MWCO 12-14 kDa)

Method

1. Obtain and weigh freeze-dried fungal powder.
2. Dissolve fungal powder in PBS.
3. Add Buffer A lysing enzyme (10 mg/mL) and incubate in water bath at 30^{o}C for 24 hr.
4. Centrifuge at 5000 rpm for 5 min. at 4^{o}C (using J25.50 rotor) to collect cells. Discard supernatant and resuspend in PBS. Centrifuge again. Repeat this until the supernatant is clear (~5 times). Add 4M guanidine thiocyanate and rock at room temperature for 12 hours/overnight *(To make 20 mL, need 9.473 g)*.
5. Centrifuge to collect pellet and wash 3 times with PBS.
6. Add 10 mL Buffer B with proteinase K (1mg/mL) and incubate in water bath for 4 hrs at 65^{o}C.
7. Centrifuge to collect pellet centrifugation and wash with PBS.
8. Resuspend in PBS.

9. Add chloroform and methanol until chloroform:methanol:aqueous is 4:2:1 (by volume). Let sit for 10 minutes to allow it to settle. Extract off lipids (bottom layer) and dispose.
10. Empty solution into beaker. Add 20 mL 6M HCl and boil for 1 hour to hydrolyze cellular components.
11. Complete a dialysis against carbon-free deionized water for 72 hours in 4°C cold room constant stirring and daily water changes.
12. Freeze dry sample. Weigh dry mass.

3.6 Kinetic modeling

Single-G

The Single-G model assumes that organic matter – in this case, fungal necromass – degrades following first order kinetics (Berner, 1964). The Single-G model presumes:

$$G_t = G_0 e^{-kt} \tag{3.1}$$

where G_0 is the initial mass of organic matter, *k* is the first-order rate constant, and G_t is the mass of organic matter remaining at time *t*. The organic matter degrades exponentially with time.

Manipulation of Equation 3.1 gives Equation 3.2:

$$\ln (G_t/G_0) = -kt \tag{3.2}$$

To calculate *k* using the Single-G model, the natural log of the relative mass remaining (G_t/G_0) was plotted versus degradation time with the y-intercept set to 0. The slope of that line is equal to the negative of the rate constant *k*.

In order to make direct comparisons to the literature, exponential rate constants were also reported. These rate constants were calculated by dividing the negative natural log of relative mass remaining at day 90 by 90 days (Fernandez and Koide, 2014). Instead of modeling the entire degradation sequence, this method looks exclusively at degradation after 90 days. These rate constants still represent first order degradation but differ slightly from those calculated by modeling the entire degradation.

Multi-G

The Multi-G model expands upon the Single-G model. It posits that there are multiple (in this case two) pools of organic carbon degrading simultaneously, following Equation 3.3:

$$G_t = G_1 e^{-k_1 t} + G_2 e^{-k_2 t} \quad (3.3)$$

where G_1 and G_2 are the mass of organic matter in the fast- and slow-degrading pools, respectively, and sum to G_0 (Westrich and Berner, 1984). G_1 and G_2 decay exponentially according to first order rate constants k_1 and k_2, respectively, where $k_1 > k_2$. Initially, the degradation of G_1 with rate constant k_1 dominates the overall degradation rate and degradation is rapid. After the majority of that pool has degraded, the overall degradation rate slows as it becomes dominated by the degradation of G_2 with slower rate constant k_2.

To calculate rate constants k_1 and k_2, the relative amount of G_1 and G_2 must also be determined. The relative mass loss is equal to the decay of the fast- and slow-degrading pools (Equation 3.4):

$$G_t/G_0 = \beta_{0,1} e^{-k_1 t} + \beta_{0,2} e^{-k_2 t} \quad (3.4)$$

where $\beta_{0,1}$ is the relative amount of the fast-degrading pool at time = 0, $\beta_{0,2}$ is the relative amount of the slow-degrading pool at time = 0, and $\beta_{0,1} + \beta_{0,2} = 1$. The natural log of mass remaining was plotted versus time, as above. Then, the data was fit with a linear trendline and it was determined visually where the linearity of the first portion of the degradation ended (14-28 days). Then, the remaining degradation was fit with a separate linear trendline. Rate constant k_1 and k_2 were approximated from the slope of the two lines. $\beta_{0,1}$

was estimated as the mass loss up to the point where the first trendline ended, and $\beta_{0,2}$ was estimated by subtracting $1 - \beta_{0,1}$. Using the estimated values for k_1, k_2, $\beta_{0,1}$, and $\beta_{0,2}$, G_t/G_0 was modeled following Equation 3.4. The model was improved by alternating changing the rate constants and the beta values to minimize the sum of the squared residuals (SSR) using Solver. The model was fit a total of eight times, at which point the difference between the SSR of one iteration and the next was less than 0.001.

3.7 Standard additions

Standard additions of fungal cell wall components to dry, ground *Fusarium avenaceum* were analyzed with thermochemolysis-gas chromatography-mass spectrometry (pyGCMS). Chitin (Sigma; isolated from shrimp shells), mannan (Sigma; isolated from *Saccharomyces cerevisiae*), ergosterol (Sigma), and lignin (alkali; Sigma) were added to analyze the response of nitrogen-containing compounds, carbohydrates, and sterols, respectively. Standards were run to determine which peaks were associated with chitin, mannan, and ergosterol. Varying amounts of standard were added to fungal tissue and ground with a Wig-L-Bug ball and mill grinder to homogenize the mixture. Each mixture was analyzed using the pyGCMS method detailed above. The amount of standard loaded onto the column was calculated using Equation 3.5:

$$Mass\ loaded\ onto\ column = Mass\ of\ sample \times \frac{Mass\ of\ standard}{Mass\ of\ standard + fungal\ tissue} \quad (3.5)$$

where mass of sample is the mass of standard and fungal tissue mixture weighed out into the pyrolysis tube, mass of standard is the mass of chitin, mannan, or ergosterol added to fungal tissue to make the standard addition mixture, and mass of standard + fungal tissue is the total mass of mixture made. Figure 3.3 demonstrates that the total N-containing, carbohydrate, and sterol response relative to total response increased as the amount of standard loaded onto column increased. This signifies that the pyGCMS method is semiquantitative.

Tables

Table 2.1 Initial melanin content of each species determined by mass of isolated melanin and comparisons to values reported in the literature.

Species	Melanin content (mg melanin g^{-1} necromass)	Method	Reference
Cenococcum geophilum	93	Isolation	This study
	174 (70 mL growth medium)	Isolation	This study
	75 (< 30 mL growth medium)	Isolation	This study
	212 – 248	Azure A assay	Fernandez & Koide, 2014
Meliniomyces bicolor – black	160	Isolation	This study
	~ 230	Azure A assay	Fernandez & Kennedy, 2018
Suillus punctipes	7	Isolation	This study
Meliniomyces bicolor – white	13	Isolation	This study
	~ 70	Azure A assay	Fernandez & Kennedy, 2018

Table 2.2 FTIR peaks identified in the carbohydrate region. Reference: Stankiewicz et al., 1998.

Wavenumber	**Characteristic**
884	Amine groups or alkene
956	Sugar groups; -OH out of plane bend
1017	Aliphatic ethers
1072	Sugar groups; combination of C-O stretching and O-H deformation; O-C-C stretching
1150	Sugar groups; C-O asymmetric stretching

Table 2.3 Comparison of degradation rate constants of various forms of organic matter. When presented, k is the published rate constant; k_1 is the rate constant of the fast-degrading pool in the Multi-G model; k_2 is the rate constant of the slow-degrading pool in the Multi-G model; k_{exp} is the rate constant from exponential fit; k_{sg} is the rate constant from Single-G model; k_{dry} is the rate constant in dry conditions; and k_{wet} is the rate constant in wet conditions.

Type	Rate constant *k*, day^{-1}	Study length	Reference
Ectomycorrhizal fungi			
Cenococcum geophilum	k_{exp} = 0.0218 k_{sg} = 0.0340 k_1 = 0.4587 k_2 = 0.0146	90 days	This study
Meliniomyces bicolor – black	k_{exp} = 0.0127 k_{sg} = 0.0146 k_1 = 0.0773 k_2 = 0.0029	90 days	This study
Suillus punctipes	k_{exp} = 0.0381 k_{sg} = 0.0432 k_1 = 0.2051 k_2 = 0.0372	90 days	This study
Meliniomyces bicolor - white	k_{exp} = 0.0279 k_{sg} = 0.0436 k_1 = 0.2805 k_2 = 0.0409	90 days	This study
Saprotrophic fungi			
Xylaria	k_{sg} = 0.167 k_1 = 0.299 k_2 = 0.0212	28 days	Bruner, 2019
Hydnotrya	k_{sg} = 0.0503	28 days	Bruner, 2019
Yeast	k_{sg} = 0.127 k_1 = 0.171 k_2 = 0.0303	28 days	Bruner, 2019
Fusarium avenaceum	k_{sg} = 0.139 k_1 = 0.183 k_2 = 0.0813	28 days	Bruner, 2019
Leaves			
Prunus pensylvanica	k = 0.0010† k_{exp} = 0.0021* (180 days) k_1 = 0.0057* (180 days) k_2 = 0.0009* (180 days)	1 year	Melillo et al., 1982
Fagus grandifolia	k = 0.0002† k_{exp} = 0.0004* (180 days) k_1 = 0.0007* (180 days) k_2 = 0.0003* (180 days)	1 year	Melillo et al., 1982

Betula papyrifera	$k = 0.0009^{\dagger}$ $k_{exp} = 0.0009$* (180 days) $k_1 = 0.0033$* (180 days) $k_2 = 0.0002$* (180 days)	1 year	Melillo et al., 1982
Fraxinus americana	$k = 0.0013^{\dagger}$ $k_{exp} = 0.0009$* (180 days) $k_1 = 0.0037$* (180 days) $k_2 = 0.0001$* (180 days)	1 year	Melillo et al., 1982
Acer rubrum	$k = 0.0012^{\dagger}$ $k_{exp} = 0.0017$* (180 days) $k_1 = 0.0033$* (180 days) $k_2 = 0.0011$* (180 days)	1 year	Melillo et al., 1982
Acer saccharum	$k = 0.0007^{\dagger}$ $k_{exp} = 0.0008$* (180 days) $k_1 = 0.0030$* (180 days) $k_2 = 0.0003$* (180 days)	1 year	Melillo et al., 1982
Cistus incanus	$k = 0.0013^{\dagger}$ $k_{exp} = 0.0012$* (60 days)	3 years	Fioretto et al., 2005
Myrtus communis	$k = 0.0021^{\dagger}$ $k_{exp} = 0.0010$* (60 days)	3 years	Fioretto et al., 2005
Quercus ilex	$k = 0.0008^{\dagger}$ $k_{exp} = 0.0014$* (90 days)	3 years	Fioretto et al., 2005
Artocarpus heterophyllus	$k_{dry} = 0.0059^{\dagger}$ $k_{wet} = 0.0064^{\dagger}$ $k_{dry,exp} = 0.0033$* (90 days) $k_{wet,exp} = 0.0068$*(90 days) $k_{dry,sg} = 0.0036$* (90 days) $k_{wet,sg} = 0.0084$* (90 days)	16 weeks	Hasanuzzaman & Hossain, 2014
Zizyphus jujuba	$k_{dry} = 0.0056^{\dagger}$ $k_{wet} = 0.0061^{\dagger}$ $k_{dry,exp} = 0.0037$* (90 days) $k_{wet,exp} = 0.0082$*(90 days) $k_{dry,sg} = 0.0039$* (90 days) $k_{wet,sg} = 0.0101$* (90 days)	16 weeks	Hasanuzzaman & Hossain, 2014
Mangifera indica	$k_{dry} = 0.0039^{\dagger}$ $k_{wet} = 0.0044^{\dagger}$ $k_{dry,exp} = 0.0021$* (90 days) $k_{wet,exp} = 0.0059$*(90 days) $k_{dry,sg} = 0.0021$* (90 days) $k_{wet,sg} = 0.0065$* (90 days)	16 weeks	Hasanuzzaman & Hossain, 2014
Litchi chinensis	$k_{dry} = 0.0024^{\dagger}$ $k_{wet} = 0.0026^{\dagger}$ $k_{dry,exp} = 0.0018$* (90 days) $k_{wet,exp} = 0.0026$*(90 days) $k_{dry,sg} = 0.0020$* (90 days) $k_{wet,sg} = 0.0029$* (90 days)	16 weeks	Hasanuzzaman & Hossain, 2014

Diatoms			
Thalassiorsira weissflogii (particulate organic carbon fraction)	k = 0.10 – 0.11	1 month	Suroy et al., 2015

† Calculated from values reported in references in units of yr^{-1}.

* Estimated from published figures. Exponential (exp) and/or Single-G (sg) rate constants are presented. Length of study analyzed included in parentheses.

Table 3.1 Codes used in compound list.

Classification	**Code**
Aliphatic	Alip
Aromatic	Aro
Carbohydrate	Carb
Nitrogen-containing	Ncont
Sterol	Ster
Unspecified	Unsp

Table 3.2 Ions and retention (RT) times used for single-ion monitoring (SIM) for pyGCMS.

ID	m/z	RT (min.)
8A Carb	75	4.39
A Carb	89	4.86
B Carb	110	5.95
2A Unsp	101	6.47
C Aro	91	6.92
D Ncont	116	8.03
E Ncont	84	8.48
1A Carb	103	8.93
8B Unsp	75	8.99
F Unsp	114	9.38
G Carb	144	10.11
8D Unsp	71	10.55
8C Unsp	87	10.61
H Aro	138	11.1
5A Unsp	74	11.13
2B Carb	123	11.51
12 Unsp	104	12.62
I Unsp / Aro	142	13.04
J Unsp	158	13.25
13A Unsp	71	13.25
13C Unsp	157	13.43
13 Aro	154	13.61
14 Aro	121	13.65
13B Unsp	97	13.67
13 Ncont	123	13.71
6A Unsp	71	14.27
14 Ncont	167	14.34
4A Aro	181	14.49
5B Unsp	98	14.63
8F Unsp	124	14.78
3A Carb	129	14.9
9A Ncont	122	15.18
K Unsp	168	15.54
1B Unsp	128	15.95
16 Ncont	144	16.11
16 Aro	135	16.11
16 Sulf	135	16.21
L Ncont	98	16.25

16A Ncont	135	16.54
2C Unsp	136	16.63
16B Ncont	154	16.65
4B Carb	129	16.66
N Carb	110	17
17 Sulf	141	17.19
8H Aro	131	17.29
5C Carb	167	17.38
18 Carb	101	17.63
17 Ncont	152	17.75
O Aro	167	18
18 Alip	168	18.03
8I Unsp	160	18.06
8J Unsp	128	18.25
P Unsp	128	18.336
Q Unsp	167	18.55
18 Aro	205	18.66
R Aro/Carb	198	18.9
S Unsp	89	18.95
8K Aro	151	19.05
19A Ncont	154	19.21
T Aro	212	19.27
19 Carb	129	19.28
19 Alip	140	19.31
5E Unsp	71	19.42
19B Ncont	154	19.57
U Carb	129	19.74
20 Ncont	154	20.07
V Carb	129	20.08
5F Carb	129	20.12
20 Aro	168	20.21
9B Aro	163	20.22
20 Unsp	154	20.37
W Carb	129	20.42
2D Alip	129	20.46
X Carb	145	20.6
5G Carb	129	20.74
20 Sulf	166	20.854
6B Carb	89	21.19
21 Ncont	154	21.23
5H Alip	152	21.35

6C Ncont	151	21.392
6D Carb	101	21.68
5I Sulf	186	22.21
Y Carb	101	22.29
3B Aro	165	22.37
Z Carb	129	23.34
23 Sulf	91	23.51
6F Carb	88	23.54
24 Unsp	71	24.11
4E Aro	161	24.2
1D Unsp	156	24.2
AA Ncont	148	25.12
5K Aro	187	25.16
AB Alip	74	25.22
3D Alip	247	25.23
AC Ncont	152	25.72
5C Alip	181	25.82
IF Alip	74	26.3
26 Ncont	182	26.3
AD Ncont	182	26.47
1H Alip	181	26.6
1I Carb	181	26.9
AF Unsp	168	27
8M Alip	74	27.32
AG Alip	87	27.32
1J Alip	327	28.315
AH Unsp	75	28.33
8N Unsp	157	28.34
8O Unsp	125	28.51
6H Alip	55	28.9
AI Alip	69	28.91
AJ Alip	87	29.32
8P Alip	264	29.56
1L Alip	87	29.6
8Q Alip	87	29.9
8R Alip	69	30.74
1M Alip	55	30.78
30 Sulf	130	30.91
5L Unsp	129	30.95
5M Unsp	98	31.08
AL Alip	87	31.23

5N Aro	241	31.99
8S Alip	69	32.6
AM Alip	69	32.61
AO Alip	74	33.07
AP Alip	67	33.36
AQ Alip	67	34.14
4G Alip	55	34.4
9D Ncont	164	34.86
35 Alip	111	35.13
1N Carb	101	36.37
8U Alip	74	36.5
4H Carb	101	36.5
37 Carb	111	36.69
9E Carb	101	36.93
4I Carb	101	37.5
37A Unsp	227	37.52
37B Unsp	154	37.911
37C Unsp	115	38
38 Alip	154	38.163
1O Carb	101	38.39
AS Carb	129	38.59
38 Sterol	267	38.66
AT Carb	88	38.85
5P Carb	88	39.15
1P Alip	143	39.68
40 Ncont	164	40.2
40 Alip	334	40.429
6I Unsp	88	40.49
5Q Unsp	329	40.69
41A Alip	325	41.09
1Q Alip	74	41.19
41A Sterol	252	41.45
41B Sterol	253	41.66
41B Alip	348	41.88
42 Alip	339	42.59
AU Alip	87	42.64
43A sterol	363	43.33
43 Alip	351	43.54
1S Alip	353	44.29
44 Unsp	220	44.45
44 Sterol	384	44.53

45A Sterol	207	45.83
AV Sterol	253	45.853
45B Sterol	326	45.94
46A Sterol	253	46.25
47A Sterol	253	47.44
47 Sterol	285	47.51
AW Sterol	207	47.524
1S Sterol	284	47.85
47C Sterol	255	47.97
AX Sterol	253	48.12
48B Sterol	255	48.82
48 Sterol	363	48.93
6J Sterol	425	50.78

Table 3.3 Comparison of exponential, Single-G, and Multi-G kinetic models and their fit to the data. Lower sum of the squared residuals (SSR) signifies a better fit. CG = *Cenococcum geophilum*; MBb = *Meliniomyces bicolor* – black; SP = *Suillus punctipes*; MBw = *Meliniomyces bicolor* – white.

	Exponential		**Single-G**		**Multi-G**		
Species	$\mathbf{k_{exp}}$	**SSR**	$\mathbf{k_{sg}}$	**SSR**	$\mathbf{k_1}$	$\mathbf{k_2}$	**SSR**
CG	0.0218	8.105	0.0340	0.978	0.4587	0.0146	0.018
MBb	0.0127	0.548	0.0146	0.117	0.0773	0.0029	0.016
SP	0.0381	5.347	0.0432	0.509	0.1955	0.0554	0.029
MBw	0.0279	8.616	0.0436	0.433	0.2805	0.0409	0.017

Table 3.4 Degradation of each species of necromass presented as relative mass remaining (mass at harvest / initial mass). CG = *Cenococcum geophilum*, MBb = *Meliniomyces bicolor* – black, SP = *Suillus punctipes*, MBw = *Meliniomyces bicolor* – white.

	Relative mass remaining			
Harvest day	**CG**	**MBb**	**SP**	**MBw**
0	0.996	0.974	0.966	0.961
1	0.643	0.994	0.818	0.776
2	0.564	0.959	0.767	0.684
4	0.417	0.849	0.631	0.576
7	0.264	0.716	0.309	0.361
14	0.202	0.573	0.107	0.267
28*	0.128	0.563	0.090	0.071
60*	0.067	0.388	0.109	0.023
90*	0.140	0.319	0.032	0.081

*Values for day 28, day 60, and day 90 calculated using average initial mass of all remaining bags on that day due to site disturbance.

Table 3.5 Average relative abundances determined with pyGCMS of the six classifications of compound (aliphatic, aromatic, carbohydrate, nitrogen-containing, sterol, and unspecified) in each species across degradation sequence. There was not enough mass of *Meliniomyces bicolor* – white after 90 days to analyze.

		Relative abundance					
Species	Harvest day	Aliphatic	Aromatic	Carbohydrate	N-containing	Sterol	Unspecified
Cenococcum geophilum	0	0.395	0.068	0.320	0.108	0.009	0.101
	1	0.411	0.033	0.493	0.038	0.010	0.015
	2	0.572	0.026	0.321	0.028	0.014	0.038
	4	0.433	0.030	0.403	0.059	0.008	0.067
	7	0.323	0.021	0.551	0.035	0.011	0.059
	14	0.305	0.029	0.526	0.057	0.021	0.062
	28	0.365	0.030	0.524	0.000	0.032	0.050
	60	0.238	0.067	0.538	0.055	0.027	0.075
	90	0.194	0.082	0.569	0.043	0.053	0.060
Meliniomyces bicolor - black	0	0.847	0.006	0.131	0.000	0.016	0.000
	1	0.885	0.000	0.108	0.000	0.008	0.000
	2	0.845	0.000	0.152	0.000	0.003	0.000
	4	0.835	0.004	0.157	0.000	0.004	0.000
	7	0.848	0.002	0.142	0.000	0.009	0.000
	14	0.792	0.012	0.181	0.000	0.011	0.003
	28	0.654	0.015	0.289	0.001	0.026	0.015
	60	0.529	0.021	0.371	0.017	0.019	0.044
	90	0.504	0.022	0.331	0.000	0.062	0.081
Suillus punctipes	0	0.524	0.026	0.344	0.050	0.026	0.030
	1	0.562	0.041	0.270	0.029	0.032	0.066
	2	0.458	0.037	0.340	0.042	0.016	0.108
	4	0.458	0.027	0.330	0.066	0.024	0.094
	7	0.199	0.044	0.548	0.018	0.055	0.146
	14	0.178	0.041	0.588	0.000	0.057	0.136
	28	0.191	0.039	0.666	0.000	0.053	0.052
	60	0.160	0.045	0.430	0.032	0.255	0.079
	90	0.279	0.064	0.380	0.051	0.179	0.047
Meliniomyces bicolor - white	0	0.568	0.012	0.387	0.016	0.010	0.007
	1	0.682	0.011	0.277	0.018	0.006	0.006
	2	0.751	0.008	0.235	0.000	0.003	0.003
	4	0.789	0.009	0.195	0.000	0.004	0.003
	7	0.468	0.024	0.447	0.000	0.005	0.055
	14	0.372	0.027	0.477	0.016	0.020	0.087
	28	0.154	0.016	0.627	0.025	0.088	0.089
	60	0.110	0.097	0.622	0.000	0.112	0.060
Soil from site	-	0.367	0.268	0.318	0.000	0.002	0.046

Table 3.6 Average percent carbon, percent nitrogen, carbon-to-nitrogen ratio, ^{13}C, and ^{15}N of each species across degradation sequence.

Species	Harvest day	%C	%N	C:N	$\delta^{13}C$	$\delta^{15}N$
Cenococcum geophilum	0	41.38	4.99	8.46	-	-
	1	45.85	4.52	10.25	-12.83	-5.70
	2	47.07	4.42	10.73	-12.92	-4.13
	4	48.10	4.44	10.87	-13.20	-1.48
	7	47.00	4.10	11.59	-14.27	-2.47
	14	50.73	4.40	11.80	-14.50	-0.41
	28	51.56	3.91	13.21	-15.14	-1.73
	60	48.82	3.88	12.59	-15.81	-3.12
	90	44.71	3.05	14.64	-17.21	-2.58
Meliniomyces bicolor - black	0	55.31	2.81	18.59	-12.80	-1.22
	1	53.60	2.93	18.84	-12.48	-2.33
	2	55.75	2.68	21.07	-12.91	-0.63
	4	53.47	2.49	21.81	-12.51	-0.07
	7	50.99	2.63	20.41	-12.31	1.25
	14	53.21	2.69	18.99	-12.07	0.04
	28	46.77	2.86	17.09	-12.34	-1.42
	60	47.13	2.87	16.75	-12.33	0.45
	90	48.81	2.87	17.03	-13.55	0.17
Suillus punctipes	0	46.42	4.92	8.67	-	-
	1	44.07	5.21	8.71	-13.18	-0.63
	2	45.31	5.24	10.38	-13.28	0.01
	4	46.56	4.39	12.18	-13.02	3.36
	7	43.19	3.81	10.45	-13.01	3.18
	14	45.02	4.50	10.45	-12.41	3.50
	28	43.78	3.44	12.97	-12.16	1.67
	60	44.89	3.86	11.62	-12.66	4.89
	90	36.36	4.20	8.65	-13.20	2.48
Meliniomyces bicolor - white	0	46.78	4.10	11.70	-12.00	-6.82
	1	51.90	3.99	12.68	-11.62	-6.69
	2	50.22	3.47	14.27	-11.78	-6.20
	4	47.16	3.01	15.95	-12.16	-3.02
	7	45.42	3.02	15.23	-11.57	-3.29
	14	47.92	2.76	19.17	-11.32	-3.46
	28	44.59	3.64	12.25	-11.40	-0.92
Soil from site	-	4.07	0.37	10.95	-26.02	3.21

Table 3.7 Average peak areas from carbohydrate region of FTIR for *Cenococcum geophilum* necromass across degradation sequence.

CG Peak Areas					
Peak	**Day 0**	**Day 7**	**Day 14**	**Day 60**	**Day 90**
884	0.867	0.026	0.081	0.108	0.758
956	3.911	1.344	1.911	2.474	2.914
1017	34.911	31.760	21.272	28.234	17.301
1072	18.811	19.073	18.523	22.921	17.626
1150	1.261	1.112	1.054	1.444	0.960
CARB SUM	59.762	53.316	42.842	55.182	39.559

Table 3.8 Average peak areas from carbohydrate region of FTIR for *Suillus punctipes* necromass across degradation sequence.

SP Peak Areas					
Peak	**Day 0**	**Day 7**	**Day 14**	**Day 60**	**Day 90**
886	0.298	0.739	0.555	0.332	0.873
958	3.768	5.792	4.776	5.880	6.734
1017	36.179	33.607	28.679	27.987	28.042
1071	22.893	20.361	20.298	19.755	17.865
1150	3.970	4.288	3.096	2.725	1.673
CARB SUM	67.110	64.786	57.404	56.679	55.188

Figures

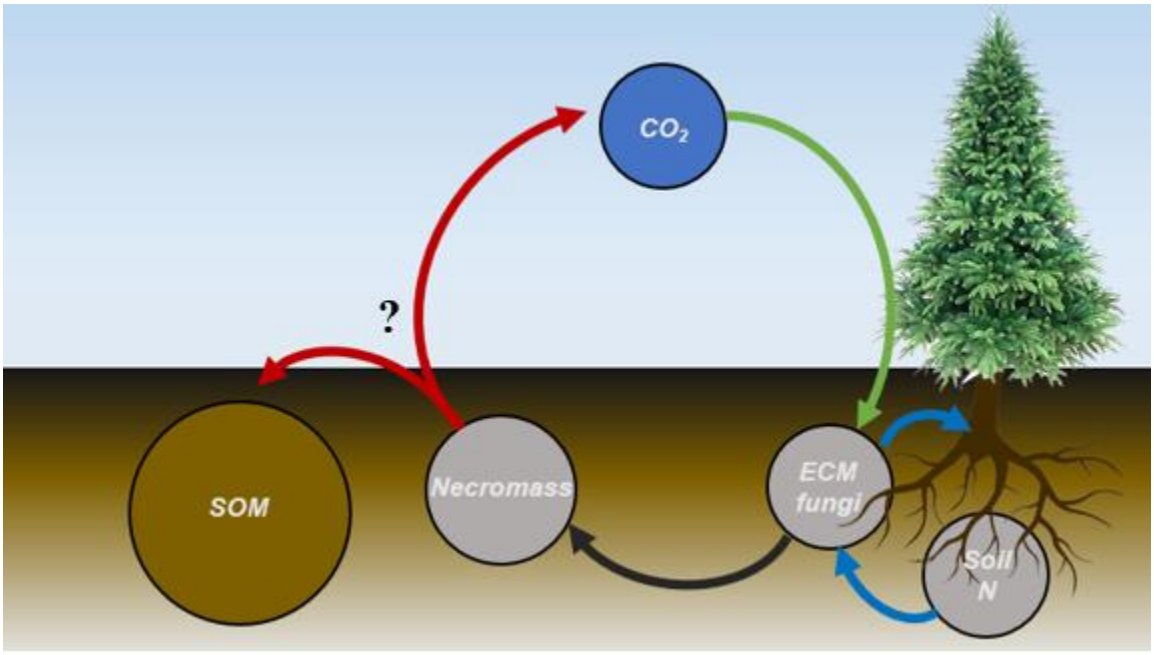

Figure 1.1/2.1 Role of ectomycorrhizal (ECM) fungi in the carbon cycle. Adapted from Fernandez et al., 2016.

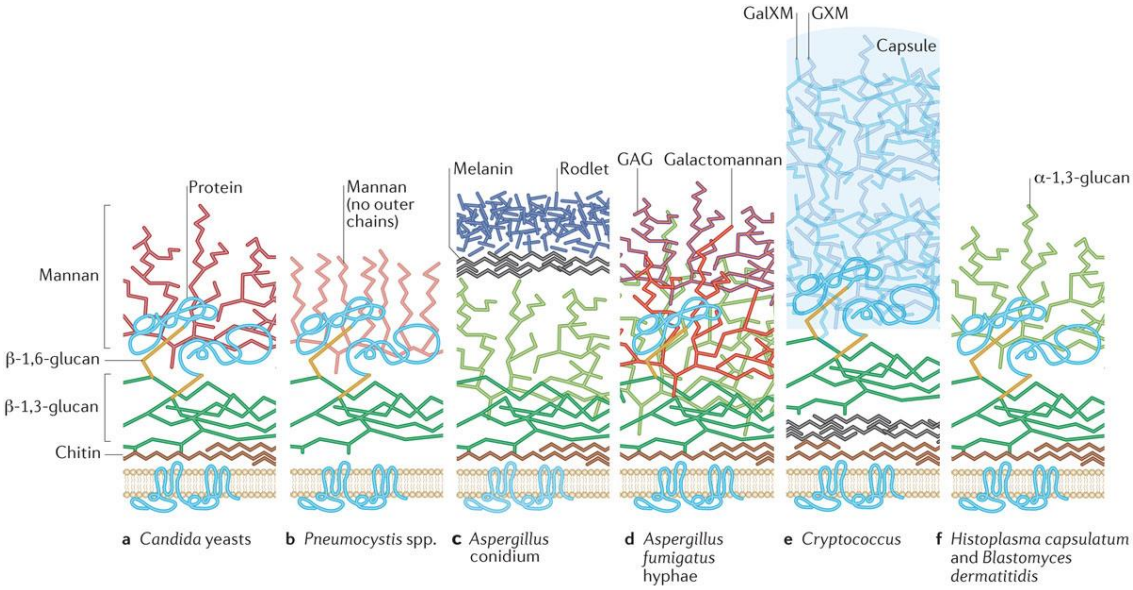

Figure 1.2/2.2 Chemical composition of fungal cell walls. From Erwig and Gow, 2016.

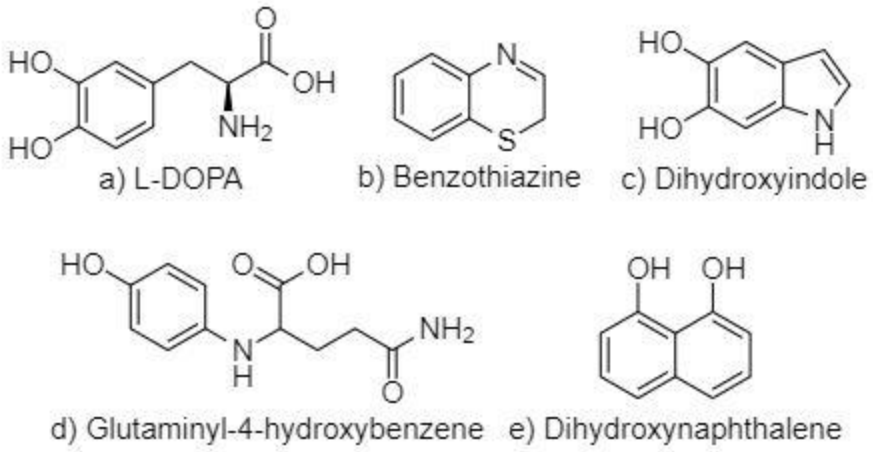

Figure 1.3/2.3 Identified monomers of melanins.

Figure 2.4 Species of ectomycorrhizal fungus studied. a) *Cenococcum geophilum* (CG); b) *Meliniomyces bicolor* – black (MBb); c) *Suillus punctipes* (SP); d) *Meliniomyces bicolor* – white (MBw). CG (93 mg melanin g^{-1} bulk) and MBb (160 mg melanin g^{-1} bulk) were "high-melanin" species. SP (7 mg melanin g^{-1} bulk) and MBw (13 mg melanin g^{-1} bulk) were "low-melanin" species.

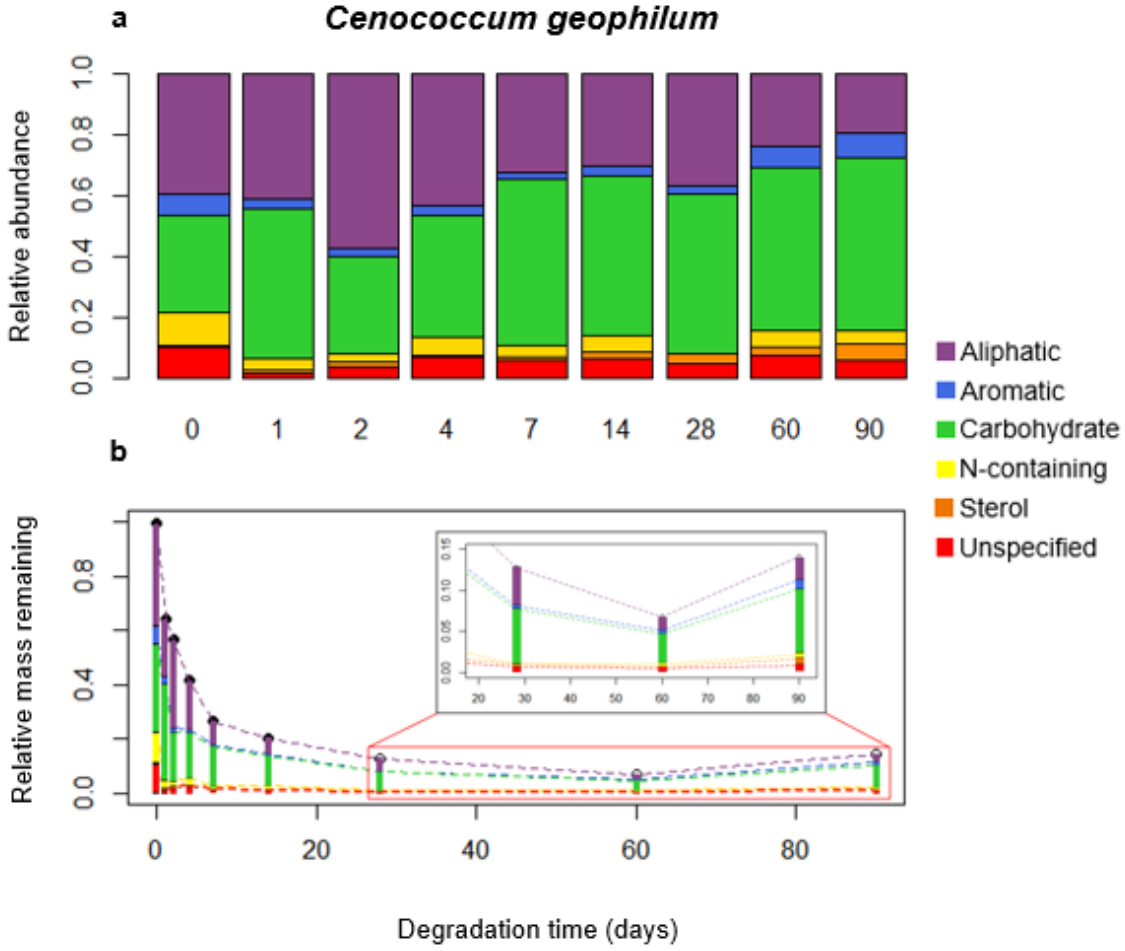

Figure 2.5 Degradation of *Cenococcum geophilum* necromass in terms of (a) chemical changes of bulk necromass and (b) degradation of each classification of compound. Lines are included to guide the eye.

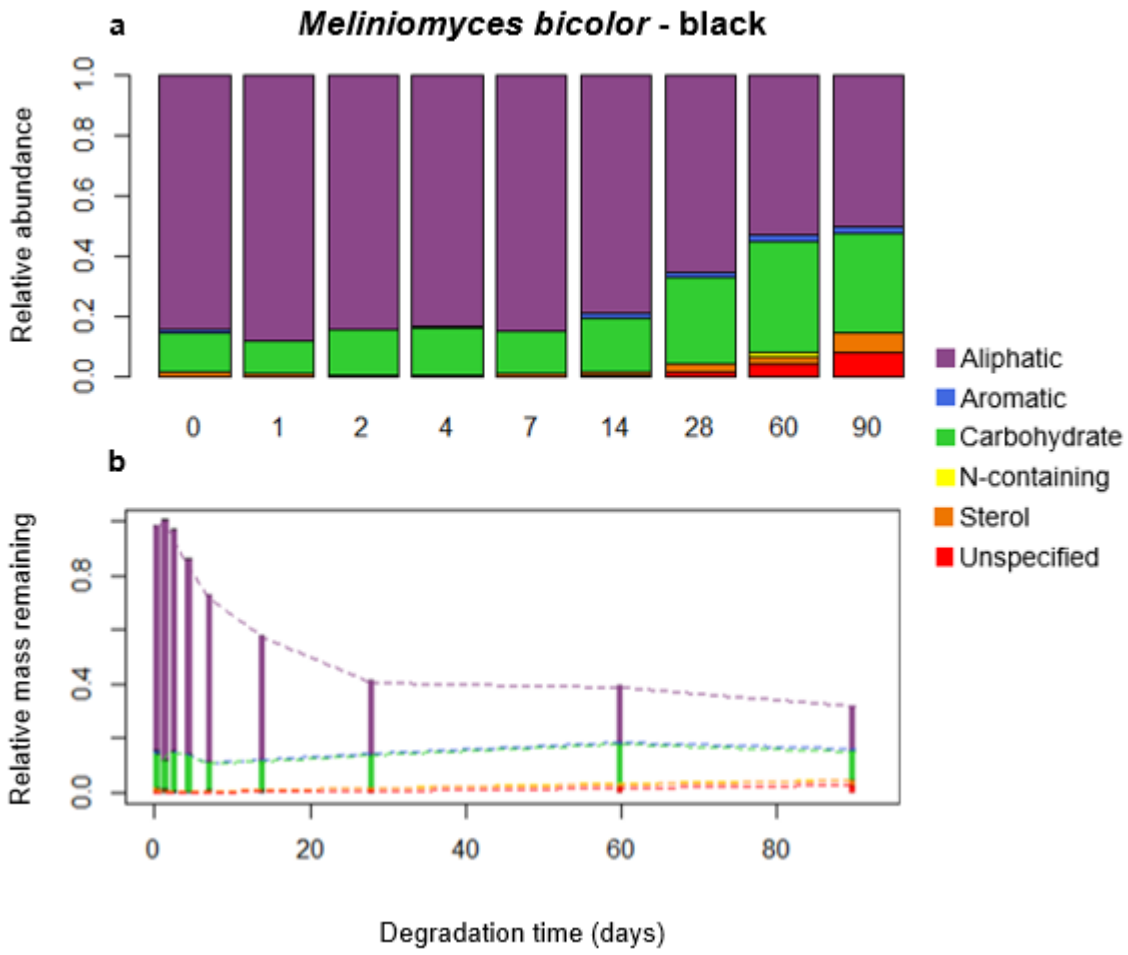

Figure 2.6 Degradation of *Meliniomyces bicolor* - black necromass in terms of (a) chemical changes of bulk necromass and (b) degradation of each classification of compound. Lines are included to guide the eye.

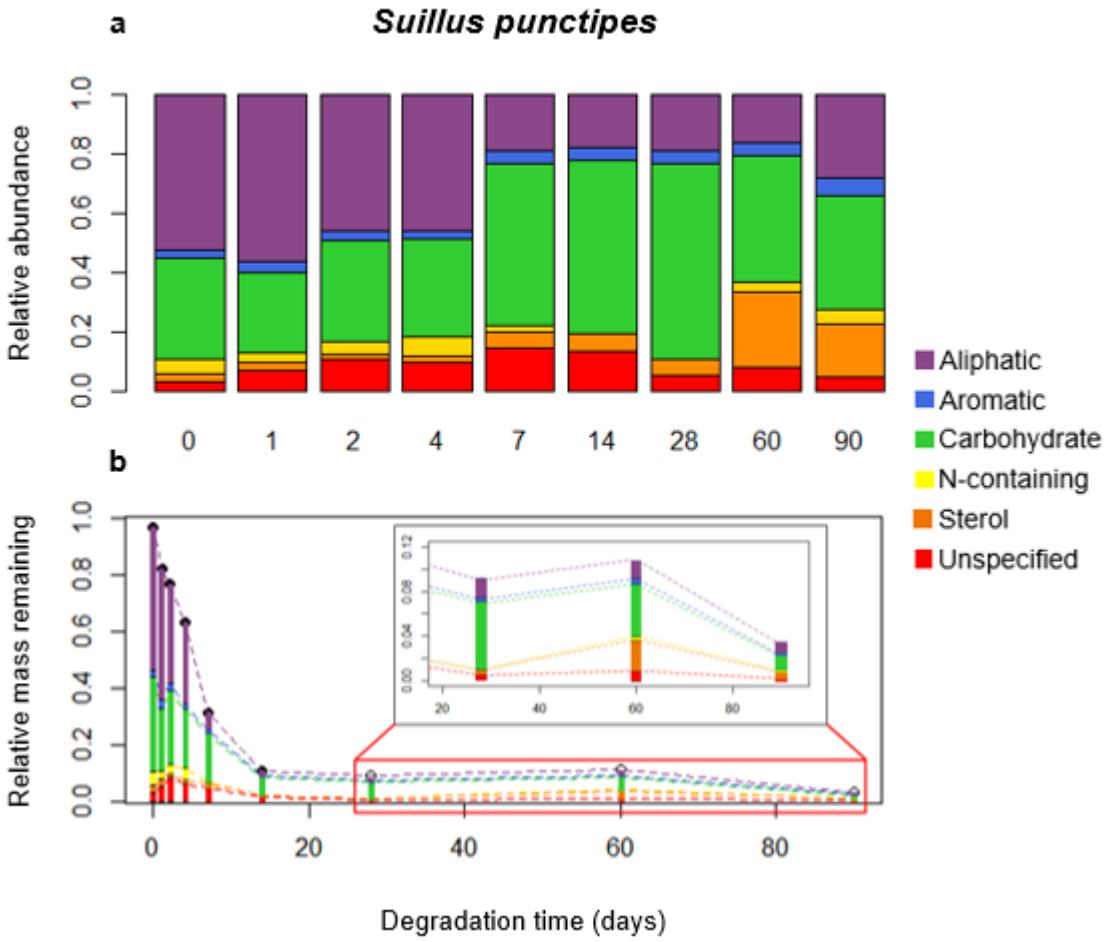

Figure 2.7 Degradation of *Suillus punctipes* necromass in terms of (a) chemical changes of bulk necromass and (b) degradation of each classification of compound. Lines are included to guide the eye.

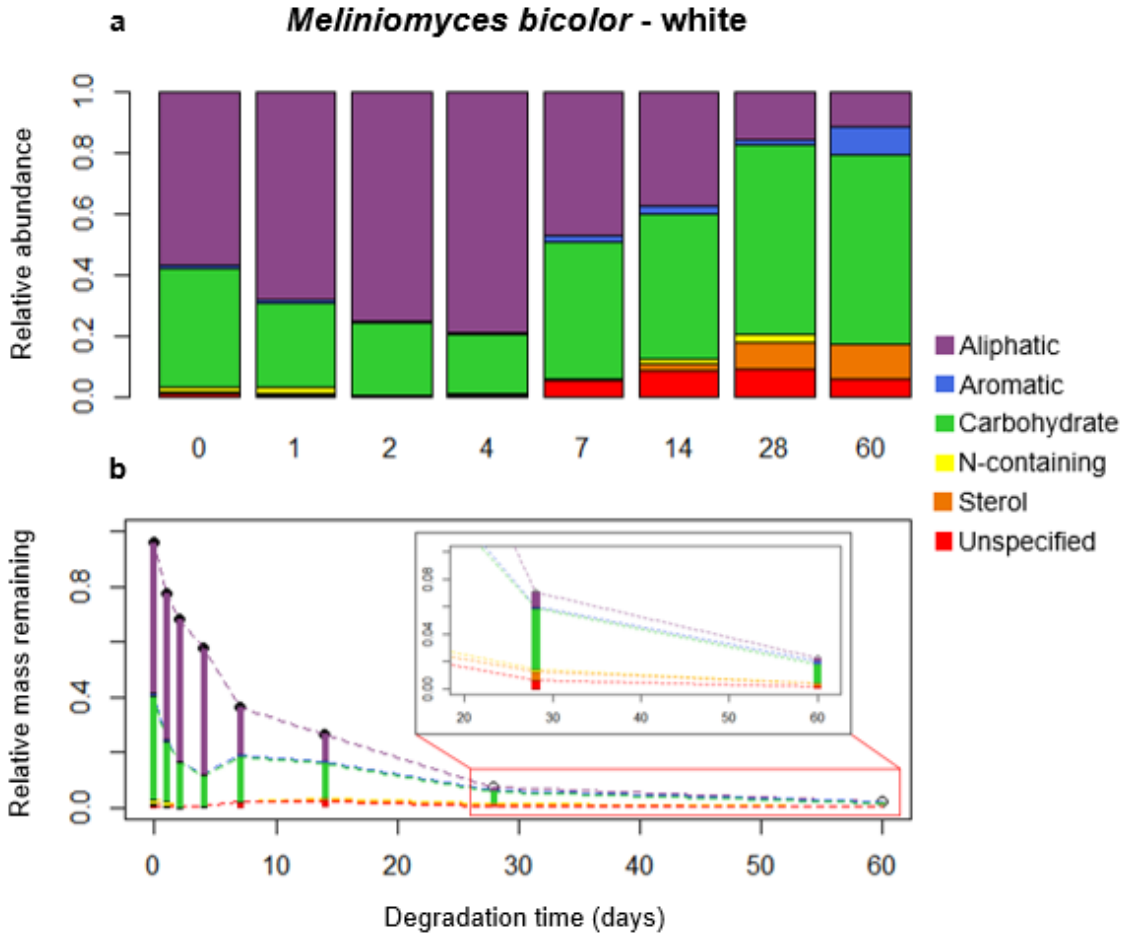

Figure 2.8 Degradation of *Meliniomyces bicolor* - white necromass in terms of (a) chemical changes of bulk necromass and (b) degradation of each classification of compound. Lines are included to guide the eye.

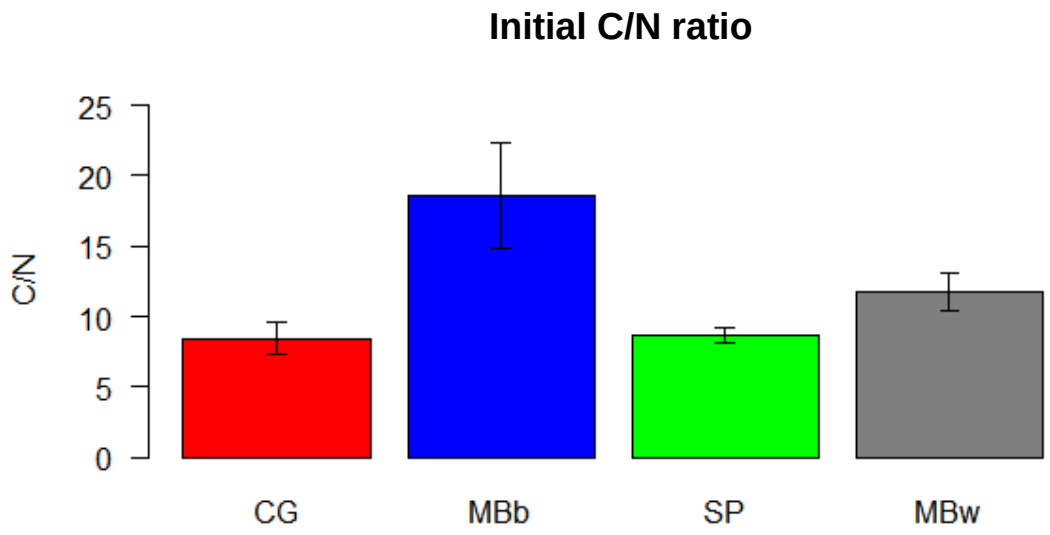

Figure 2.9 Ratio of organic carbon to nitrogen in undegraded necromass of each species. The C/N ratio of MBb necromass is significantly higher than the other three species ($p < 0.0001$). Error bars show standard deviation. CG = *Cenococcum geophilum*, MBb = *Meliniomyces bicolor* – black, SP = *Suillus punctipes*, MBw = *Meliniomyces bicolor* – white.

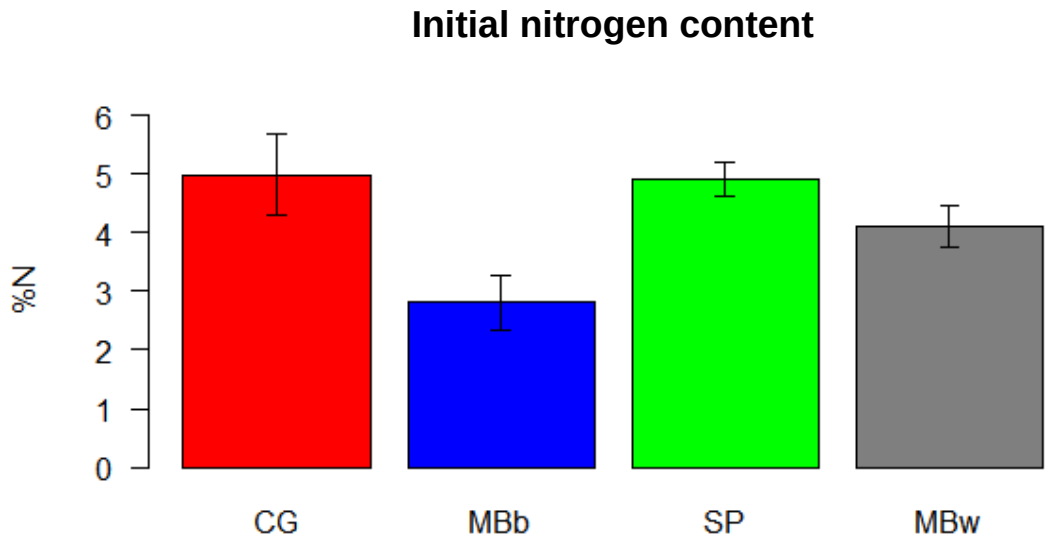

Figure 2.10 Initial nitrogen content of each species determined by elemental analysis. MBb contains significantly less nitrogen than the other three species ($p < 0.0005$). Error bars show standard deviation. CG = *Cenococcum geophilum*, MBb = *Meliniomyces bicolor* – black, SP = *Suillus punctipes*, MBw = *Meliniomyces bicolor* – white.

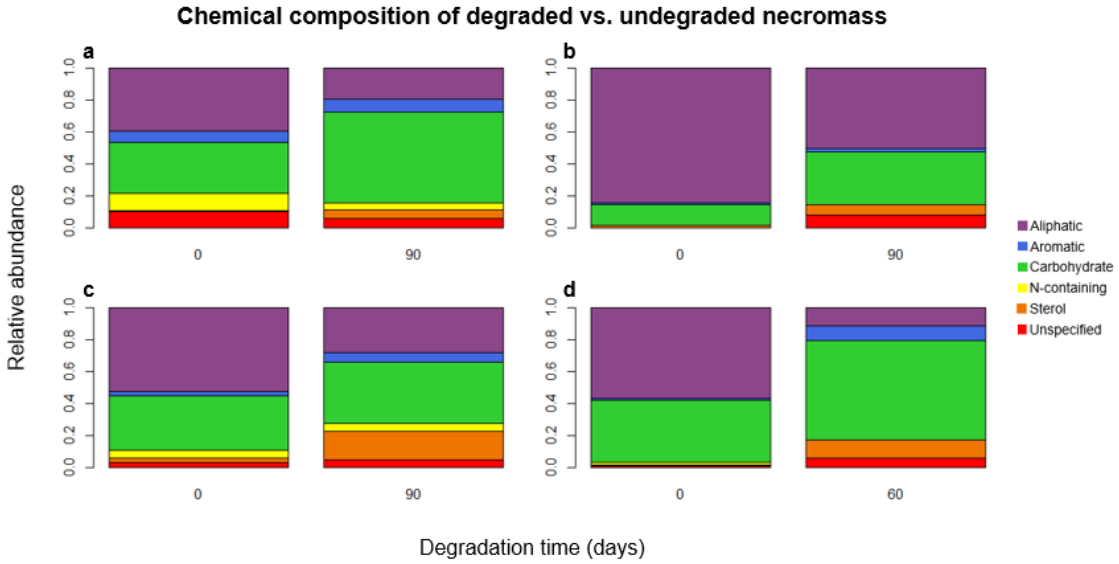

Figure 2.11 Chemical comparison of degraded (day 60 or day 90) and undegraded (day 0) necromass. (a) *Cenococcum geophilum*; (b) *Meliniomyces bicolor* – black; (c) *Suillus punctipes*; (d) *Meliniomyces bicolor* – white.

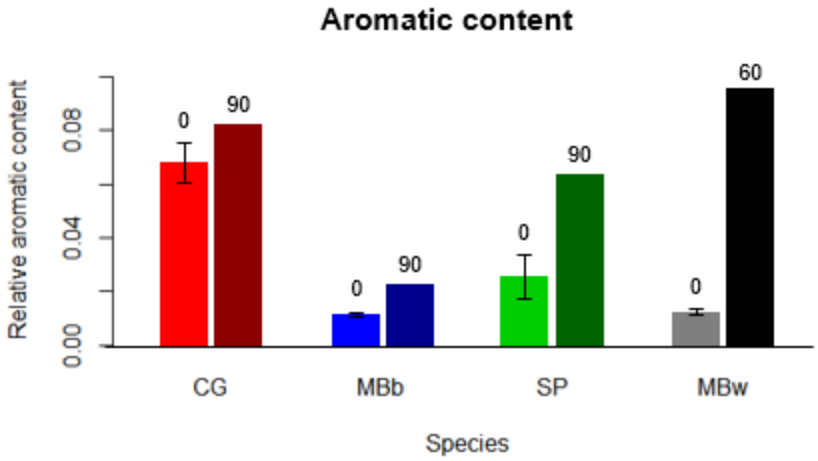

Figure 2.12 Relative aromatic content of degraded and undegraded necromass. Error bars show standard deviation. Number above bar indicates days of degradation. CG = *Cenococcum geophilum*; MBb = *Meliniomyce bicolor* – black; SP = *Suillus punctipes*; MBw = *Meliniomyces bicolor* – white.

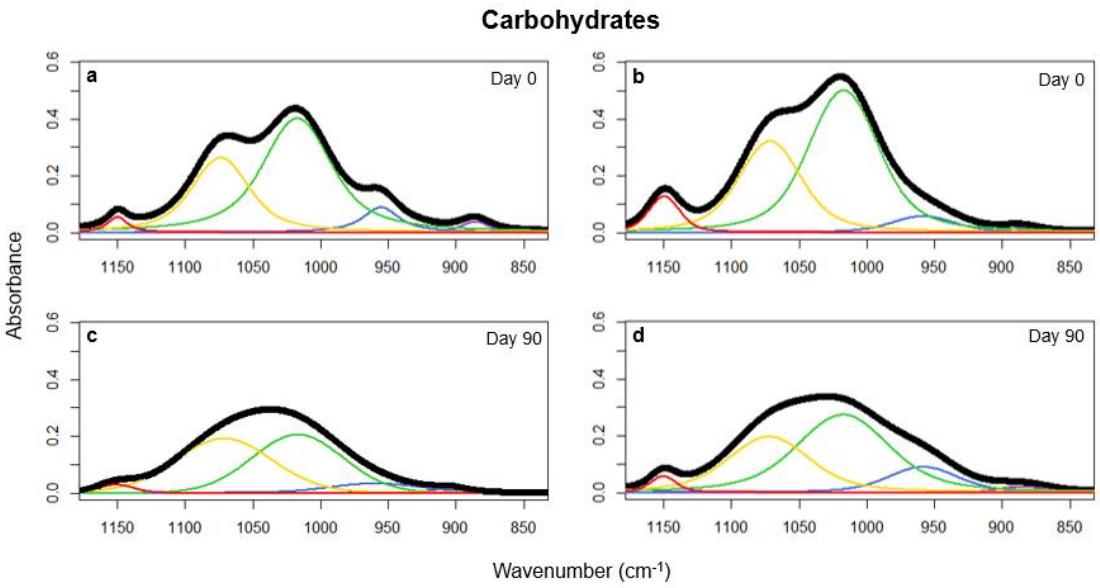

Figure 2.13 FTIR spectra of the carbohydrate region of CG and SP at days 0 and 90. Peaks deconvoluted using PeakFit software. (a) *Cenococcum geophilum*, day 0; (b) *Suillus punctipes*, day 0; (c) *Cenococcum geophilum*, day 90; (d) *Suillus punctipes*, day 90.

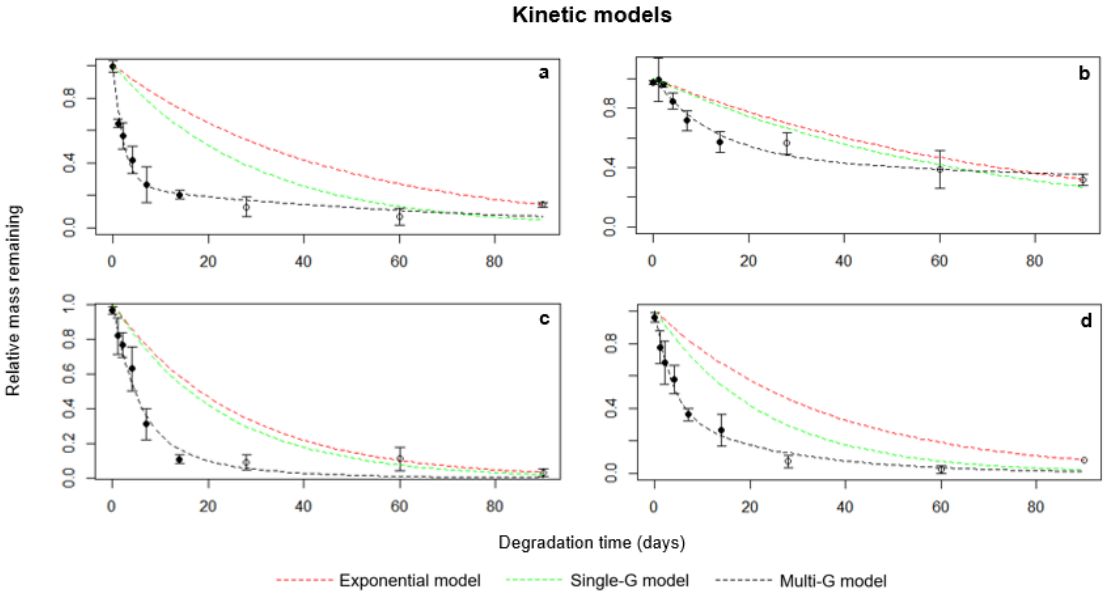

Figure 2.14 Degradation of necromass from (a) *Cenococcum geophilum*; (b) *Meliniomyces bicolor* – black; (c) *Suillus punctipes*; and (d) *Meliniomyces bicolor* – white. Error bars show standard deviation. Lines show exponential, Single-G, and Multi-G fits; see Table 1 for rate constants.

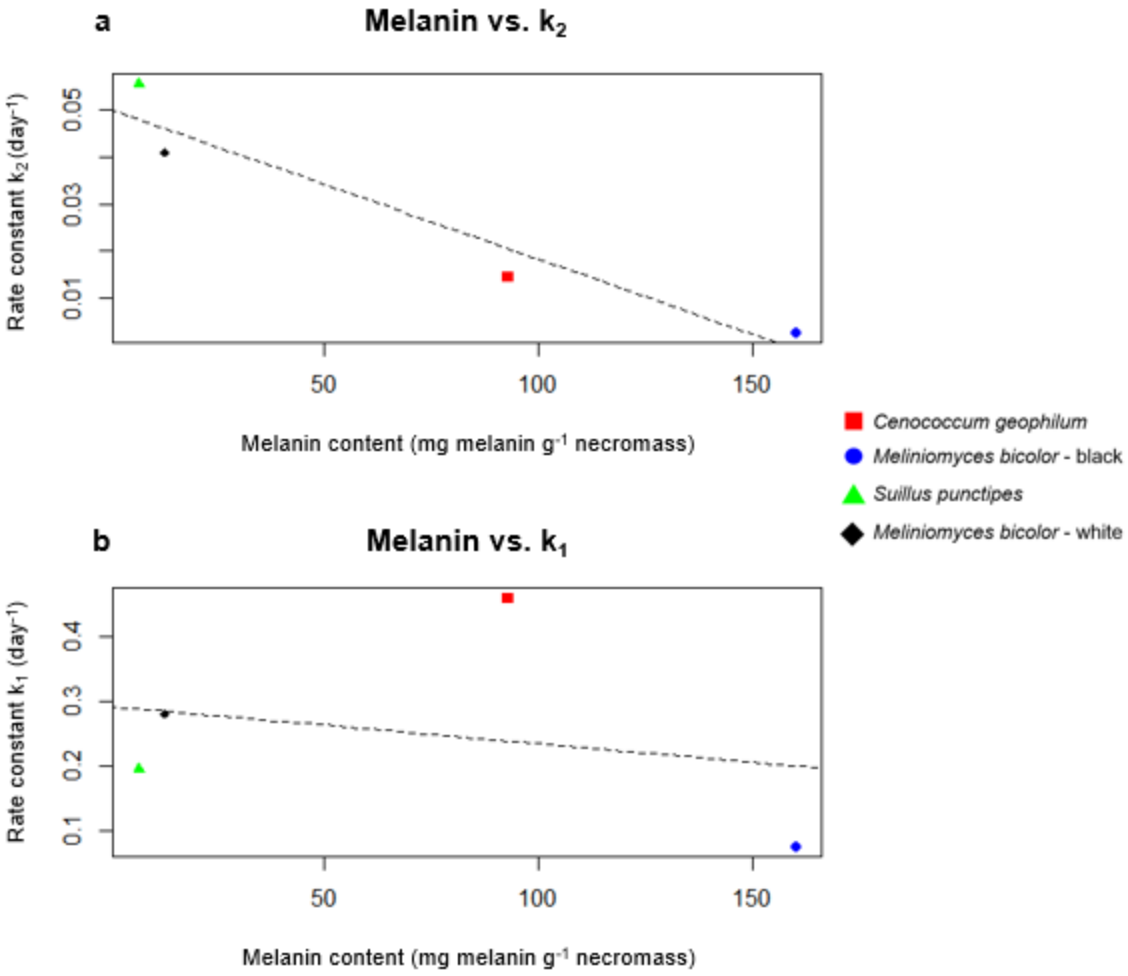

Figure 2.15 Melanin content (mg melanin g^{-1} necromass) versus rate constant for (a) slow-degrading pool, k_2 (day^{-1}) ($R^2 = 0.92$; $p < 0.05$) and (b) fast-degrading pool, k_1, ($R^2 = 0.07$, $p > 0.70$).

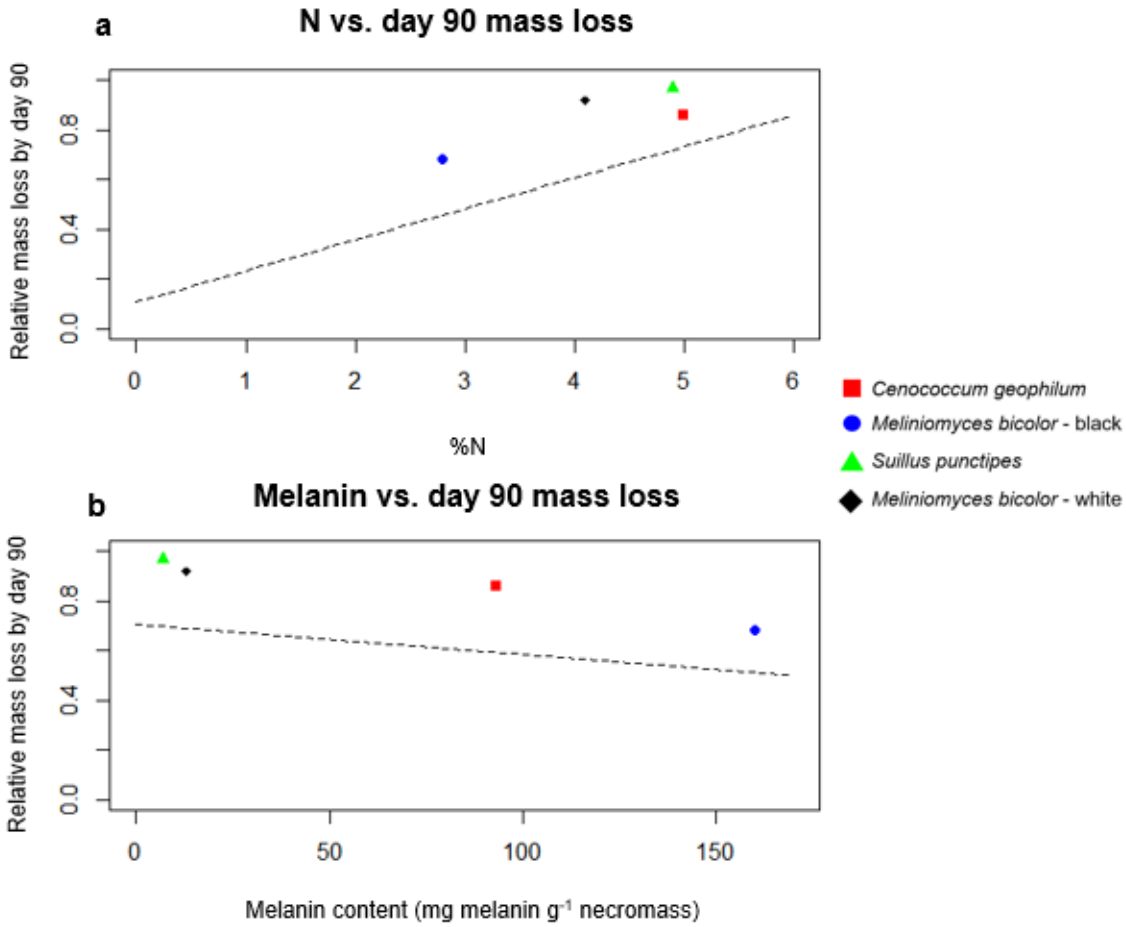

Figure 2.16 Relationships between average mass loss by day 90 and a) nitrogen content (%N) and b) melanin content (mg melanin g^{-1} necromass). Lines are best fit lines from data published by Fernandez & Koide (2014). (a) % mass loss = 0.125 *(%N) + 0.107. (b) % mass loss = -0.00121*(melanin content) + 0.705.

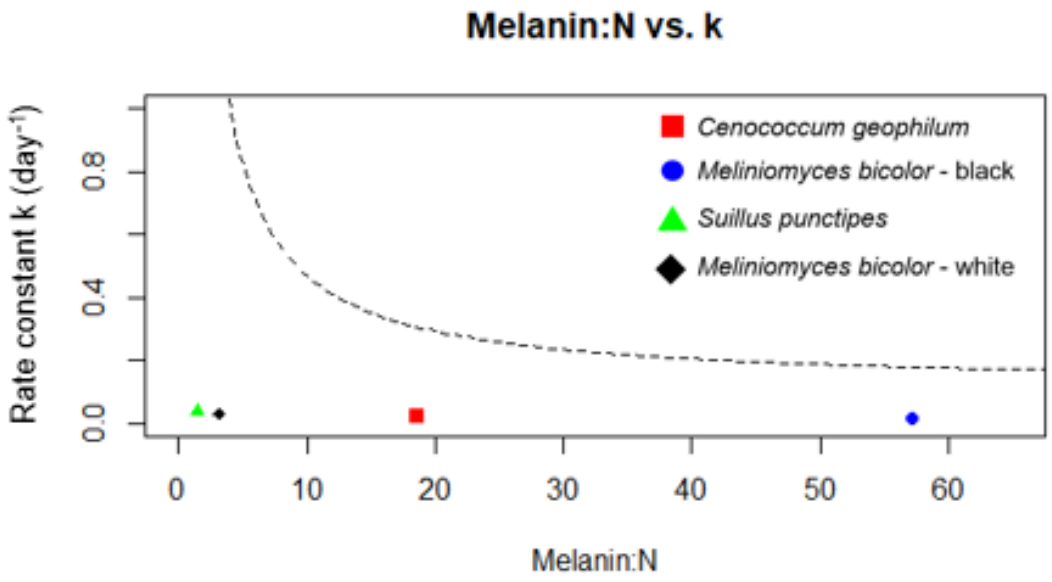

Figure 2.17 Ratio of melanin: N (mg melanin g^{-1} necromass / %N) vs. rate constant k_{exp} (day^{-1}). Line is fit published by Fernandez & Koide (2014): $k = 0.117 + 3.52/$ (melanin: N).

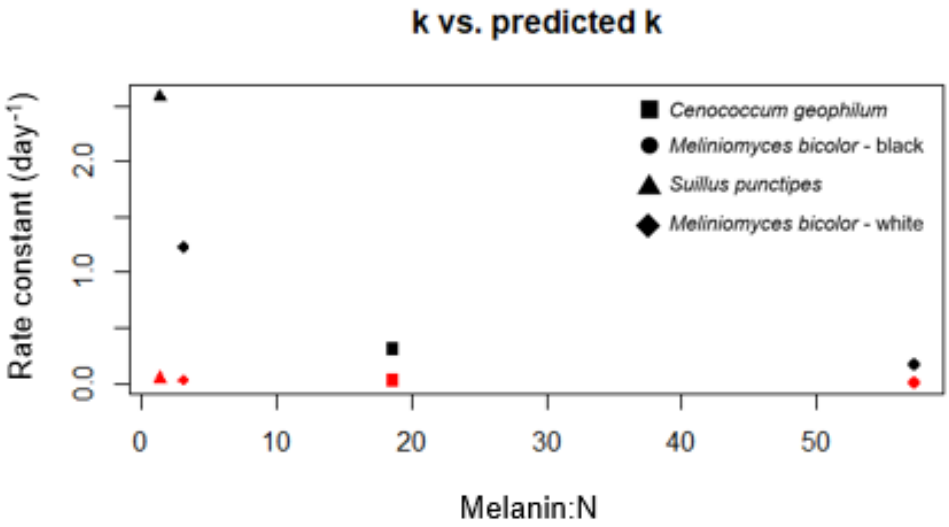

Figure 2.18 Observed rate constant k_{exp} (black) and predicted rate constant k (red). Predicted k calculated from melanin: N based on relationship observed by Fernandez & Koide (2014): $k = 0.117 + 3.52/$ (melanin: N).

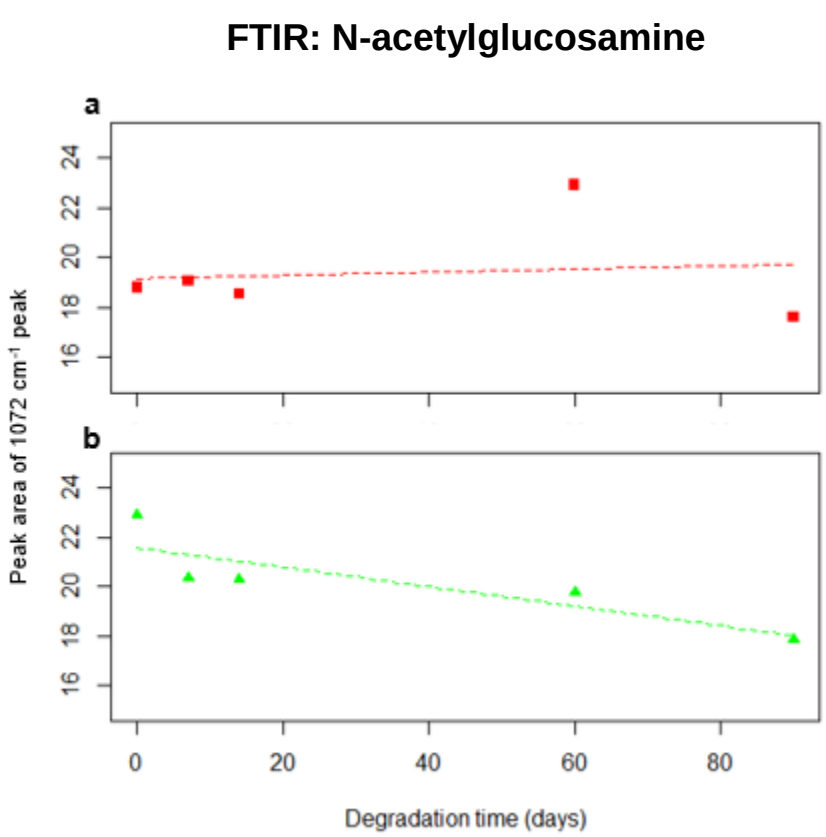

Figure 2.19 Peak area of N-acetylglucosamine peak (1072 cm^{-1}) in (a) *Cenococcum geophilum* necromass (R^2 = 0.01, p > 0.8) and (b) *Suillus punctipes* necromass (R^2 = 0.73, p < 0.1).

Figure 3.1 Additional field site information. (a) Aerial view of site; (b) example of a plot with meter stick for reference; (c) mesh litter bag containing necromass attached to an identification tag; (d) bag buried under the litter layer; (e) bag removed from the soil and detached from identification tag by an unidentified animal.

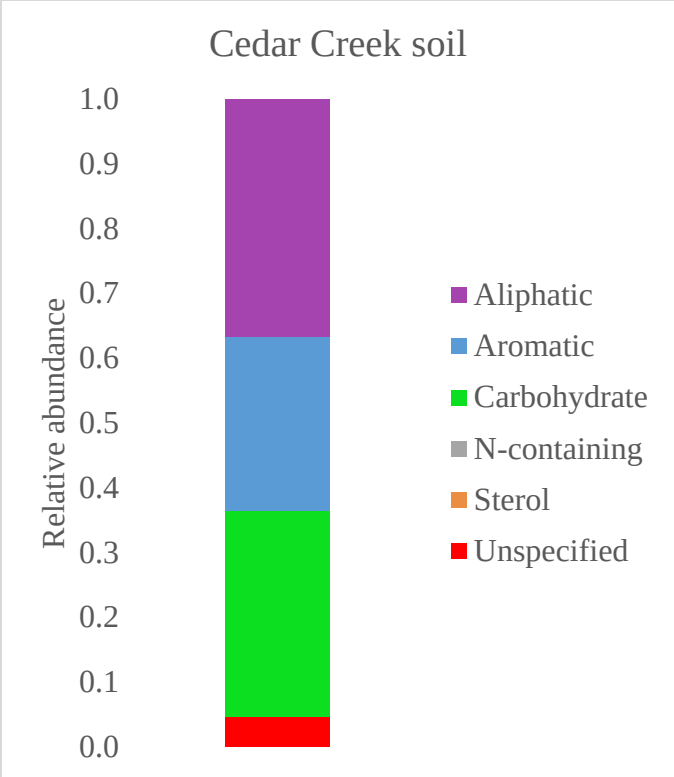

Figure 3.2 Thermochemolysis-gas chromatography-mass spectrometry (pyGCMS) characterization of soil from field site.

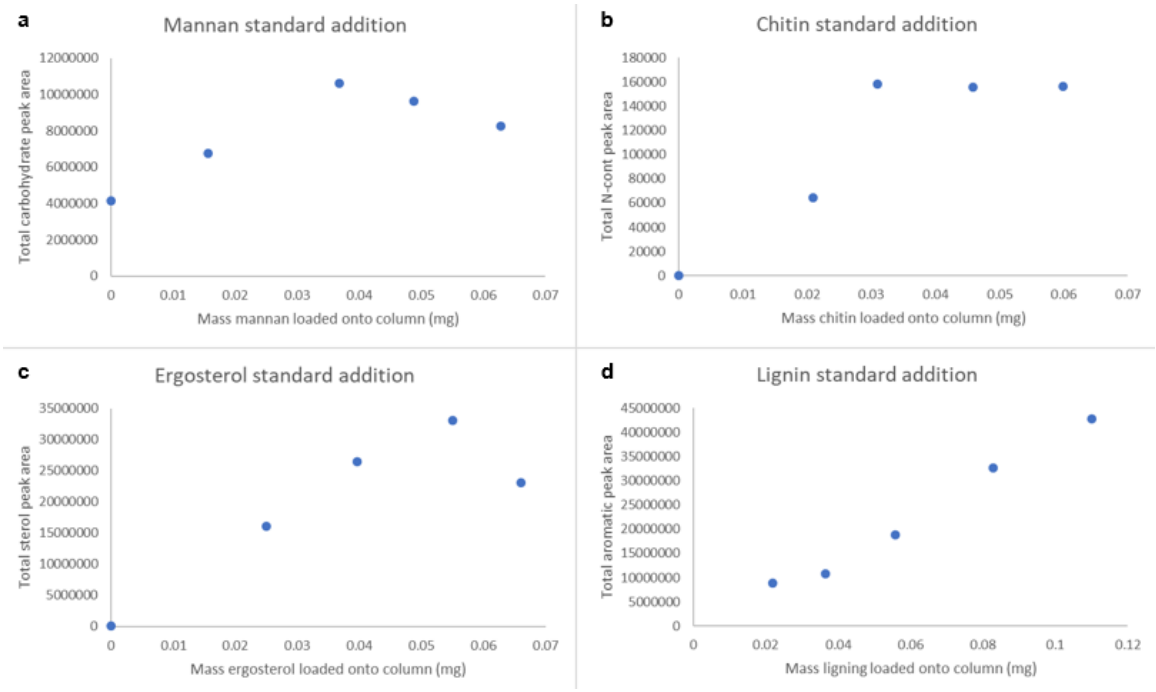

Figure 3.3 Response (raw peak area) of standard additions of (a) mannan, (b) chitin, (c) ergosterol, and (d) lignin to *Fusarium avenaceum* necromass using thermochemolysis-GCMS.

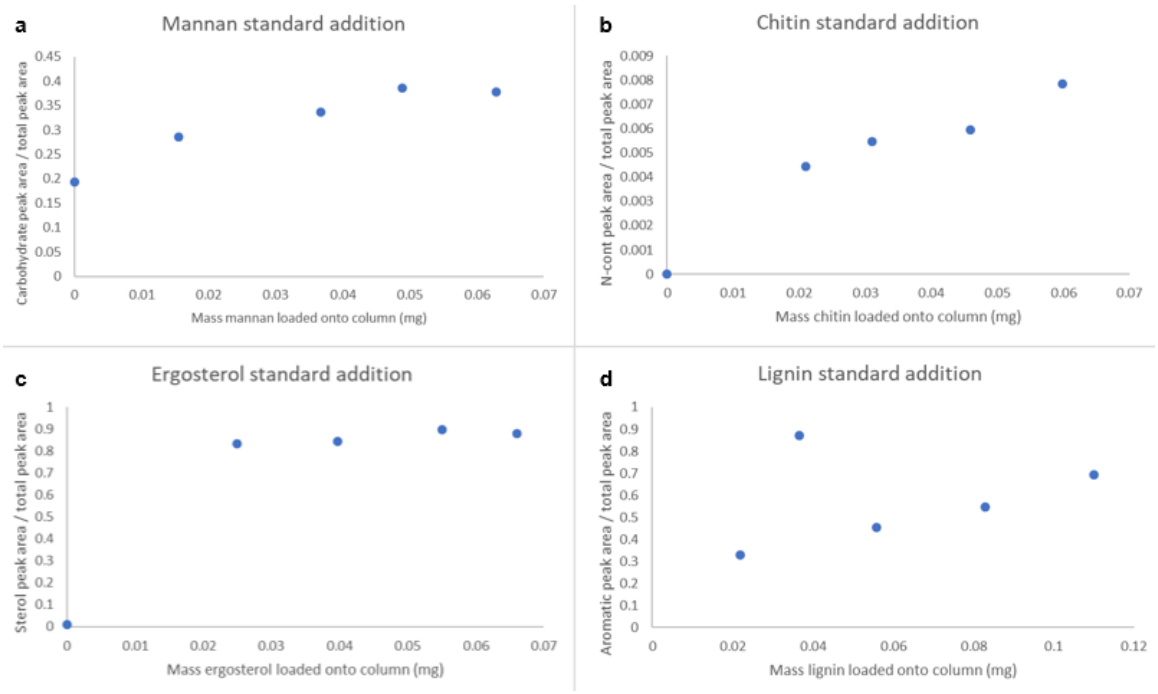

Figure 3.4 Response (relative peak area) of standard additions of (a) mannan, (b) chitin, (c) ergosterol, and (d) lignin to *Fusarioum avenaceium* necromass using thermochemolysis-GCMS.

References

Baath, E., Nilsson, L.O., Goransson, H., Wallander, H., 2004. Can the extent of degradation of soil fungal mycelium during soil incubation be used to estimate ectomycorrhizal biomass in soil? Soil Biology and Biochemistry 36, 2105–2109.

Bartnicki-Garcia, S., 1968. Cell wall chemistry, morphogenesis, and taxonomy of fungi. Annual Review of Microbiology 88–108.

Baskaran, P., Hyvönen, R., Berglund, S.L., Clemmensen, K.E., Ågren, G.I., Lindahl, B.D., Manzoni, S., 2017. Modelling the influence of ectomycorrhizal decomposition on plant nutrition and soil carbon sequestration in boreal forest ecosystems. New Phytologist 213, 1452–1465.

Berner, R.A., 1964. An idealized model of dissolved sulfate distribution recent sediments in. Geochimica et Cosmochimica Acta 28, 1497–1503.

Bruner, V.J., 2019. Chemical Characterization of the Degradation of Necromass from Four Ascomycete Fungi: Implications for Soil Organic Carbon Turnover and Storage.

Bull, A.T., 1970. Inhibition of Polysaccharases in Relation by Melanin: to Mycolysis Enzyme Inhibition A role for melanin in the resistance of fungi to microbial lysis is evident from recent reports. The present investigation was dire. Archives of Biochemistry and Biophysics 345–356.

Butler, M.J., Day, A.W., 1998. Fungal melanins: a review. Canadian Journal of Microbiology 44, 1115–1136.

Calderon, F.J., Mccarty, G.W., Reeves, J.B., 2006. Pyrolisis-MS and FT-IR analysis of fresh and decomposed dairy manure. Journal of Analytical and Applied Pyrolysis 76, 14–23.

Certano, A.K., Fernandez, C.W., Heckman, K.A., Kennedy, P.G., 2018. The afterlife effects of fungal morphology: Contrasting decomposition rates between diffuse and rhizomorphic necromass. Soil Biology and Biochemistry 126, 76–81.

Clemmensen, K.E., Bahr, A., Ovaskainen, O., Dahlberg, A., Ekblad, A., Wallander, H., Stenlid, J., Finlay, R.D., Wardle, D.A., Lindahl, B.., 2013. Roots and Associated Fungi Drive Long-Term Carbon Sequestration in Boreal Forest. Science 339, 1615–1618.

Çoban-Yıldız, Y., Fabbri, D., Tartari, D., Tuğrul, S., Gaines, A.., 2000. Application of pyrolysis–GC/MS for the characterisation of suspended particulate organic matter in the Mediterranean Sea: a comparison with the Black Sea. Organic Geochemistry 31, 1627–1639.

Coelho, R.R.R., Sacramento, D.R., Linhares, L.F., 1997. Amino sugars in fungal melanins and soil humic acids. European Journal of Soil Science 48, 425–429.

Conant, R.T., Ryan, M.G., Agren, G.I., Birge, H.E., Davidson, E.A., Eliasson, P.E., Evans, S.E., Frey, S.D., Kirschbaum, F., Lavallee, J.M., Leifeld, J., Parton, W.J., Steinweg, J.M., Wallenstein, M.D., Wetterstedt, M.J.A., Bradford, M.A., 2011. Temperature and soil organic matter decomposition rates – synthesis of current knowledge and a way forward. Global Change Biology 3392–3404.

Cotrufo, M.F., Ineson, P., Roberts, J.D., 1995. Decomposition of birch leaf litters with varying C-to-N ratios. Soil Biology and Biochemistry 27, 1219–1221.

D'Ischia, M., Wakamatsu, K., Briganti, S., Kovacs, D., Meredith, P., Pezzella, A., Sarna,

T., Simon, J.D., Ito, S., 2013. International federation of pigment cell societies · society for melanoma research pigment cell & melanoma. Pigment Cell & Melanoma Research 26, 616–633.
Davidson, E.A., Janssens, I.A., 2006. Temperature sensitivity of soil carbon decomposition and feedbacks to climate change. Nature 440, 165–173.
Drake, B.G., Gonzàlez-Meler, M.A., Long, S.P., 1997. More Efficient Plants: A Consequence of Rising Atmospheric CO2? Annual Reviews of Plant Physiology 48, 609–639.
Drigo, B., Anderson, I.C., Kannangara, G.S.K., Cairney, J.W.G., Johnson, D., 2012. Rapid incorporation of carbon from ectomycorrhizal mycelial necromass into soil fungal communities. Soil Biology and Biochemistry 49, 4–10.
Dufour-Tremblay, G., Levesque, E., Boudreau, S., 2012. Dynamics at the treeline : differential responses of Picea mariana and Larix laricina to climate change in eastern subarctic Quebec. Environmental Research Letters 7, 1–10.
Dusenge, M.E., Duarte, A.G., Way, D.A., 2018. Tansley review Plant carbon metabolism and climate change: elevated CO 2 and temperature impacts on photosynthesis , photorespiration and respiration. New Phytologist 32–49.
Elliott, E.T., Coleman, D.C., 1988. Let the Soil Work for Us. Ecological Bulletins 23–32.
Erwig, L.P., Gow, N.A.R., 2016. Interactions of fungal pathogens with phagocytes. Nature Reviews Microbiology 14, 163–176.
Feofilova, E.P., 2010. The Fungal Cell Wall : Modern Concepts of Its Composition 79, 711–720.
Fernandez, C.W., Heckman, K., Kolka, R., Kennedy, P.G., 2019. Melanin mitigates the accelerated decay of mycorrhizal necromass with peatland warming. Ecology Letters.
Fernandez, C.W., Kennedy, P.G., 2018. Melanization of mycorrhizal fungal necromass structures microbial decomposer communities. Journal of Ecology 106, 468–479.
Fernandez, C.W., Koide, R.T., 2014. Initial melanin and nitrogen concentrations control the decomposition of ectomycorrhizal fungal litter. Soil Biology and Biochemistry 77, 150–157.
Fernandez, C.W., Koide, R.T., 2013. The function of melanin in the ectomycorrhizal fungus *Cenococcum geophilum* under water stress. Fungal Ecology 6, 479–486.
Fernandez, C.W., Koide, R.T., 2012. The role of chitin in the decomposition of ectomycorrhizal fungal litter. Ecology 93, 24–28.
Fernandez, C.W., Langley, J.A., Chapman, S., Mccormack, M.L., Koide, R.T., 2016. The decomposition of ectomycorrhizal fungal necromass. Soil Biology and Biochemistry 93, 38–49.
Fioretto, A., Nardo, C. Di, Papa, S., Fuggi, A., 2005. Lignin and cellulose degradation and nitrogen dynamics during decomposition of three leaf litter species in a Mediterranean ecosystem 37, 1083–1091.
Focher, B., Naggi, A., Torri, G., Cosani, A., Terbojevieh, M., 1992. Chitosans from Euphausia superba . 2 : Characterization of solid state structure 18, 43–49.
Follett, R.F., Paul, E.A., Pruessner, E.G., 2007. Soil carbon dynamics during a long-term incubaton study involvine 13C and 14C measurements. Publications from USDA-ARS/UNL Faculty.
Frank, B. 1894. Die bedeutung der mykorhiza pilze fur die gemeine Kiefer.

Forstwissenschaftliches Centralblatt. 16: 185–190.
Godbold, D.L., Hoosbeek, M.R., Lukac, M., Cotrufo, M.F., Janssens, I.A., Ceulemans, R., Polle, A., Velthorst, E.J., Scarascia-Mugnozza, G., De Angelis, P., Miglietta, F., Peressotti, A., 2006. Mycorrhizal hyphal turnover as a dominant process for carbon input into soil organic matter. Plant and Soil 281, 15–24.
Hasanuzzaman, M., Hossain, M., 2014. Leaf Litter Decomposition and Nutrient Dynamics Associated with Common Horticultural Cropland Agroforest Tree Species of Bangladesh. International Journal of Forestry Research 1–10.
Hassink, J., 1997. The capacity of soils to preserve organic C and N by their association with clay and silt particles 77–87.
Henson, J.M., Butler, M.J., Day, A.W., 1999. The Dark Side of the Mycelium: Melanins of Phytopathogenic Fungi. Annual Review of Phytopathology 447–471.
Hobbie, E.A., 2006. Carbon allocation to ectomycorrhizal fungi correlates with belowground allocation in culture studies. Ecology 87, 563–569.
Högberg, M.N., Högberg, P., 2002. Extramatrical ectomycorrhizal mycelium contributes one-third of microbial biomass and produces, together with associated roots, half the dissolved organic carbon in a forest soil. New Phytologist 154, 791–795.
Ito, S., Fujita, K., 1984. Microanalysis of Eumelanin and Pheomelanin in Hair and Melanomas Chemical Degradation and Liquid Chromatography'. Analytical Biochemistry 527–536.
Jobbagy, E.G., Jackson, R.B., 2000. The Vertical Distribution of Soil Organic Carbon and Its Relation to Climate and Vegetation the vertical distribution of soil organic carbon and its ecological applications, 10, 423–436.
Johnson, N.C., Graham, J.H., Smith, F.A., 1997. Functioning of mycorrhizal associations along the mutualism-parasitism continuum. New Phytologist 135, 575–586.
Joint Genome Institute, 2019. Meliniomyces bicolor.
Kallenbach, C.M., Frey, S.D., Grandy, A.S., 2016. Direct evidence for microbial-derived soil organic matter formation and its ecophysiological controls. Nature Communications 7, 1–10.
Karberg, N.J., Scott, N.A., Giardina, C.P., 2008. Methods for Estimating Litter Decomposition, in: Field Measurements for Forest Carbon Monitoring. pp. 103–111.
Kennedy, P.G., Mielke, L.A., Nguyen, N.H., 2018. Ecological responses to forest age , habitat , and host vary by mycorrhizal type in boreal peatlands. Mycorrhiza 28, 315–328.
Killingbeck, K.T., Smith, D.L., Marzolof, G.R., 1982. Chemical Changes in Tree Leaves During Decomposition in a Tallgass Prairie Stream. Ecology 63, 585–589.
Kögel-Knabner, I., 2002. The macromolecular organic composition of plant and microbial residues as inputs to soil organic matter: Fourteen years on. Soil Biology and Biochemistry 105, 139–162.
Koide, R.T., Malcolm, G.M., 2009. N concentration controls decomposition rates of different strains of ectomycorrhizal fungi. Fungal Ecology 2, 197–202.
Kuo, M., Alexander, M., 1967. Inhibition of the Lysis of Fungi by Melanins. Journal of Bacteriology 94, 624–629.
Lakhanpal, T.N., 2000. Ectomycorrhiza - An Overview 101–118.
Lal, R., 2004. Soil Carbon Sequestration Impacts on Global Climate Change and Food Security. Science 304, 1623–1628.

Langley, J.A., Hungate, B.A., 2003. Mycorrhizal Controls on Belowground Litter Quality 84, 2302–2312.
Melillo, J.M., Aber, J.D., Muratore, J.F., 1982. Nitrogen and Lignin Control of Hardwood Leaf Litter Decomposition Dynamics. Ecology 63, 621–626.
Moss, P., 2017. Adapting to Climate Change in Minnesota: 2017 Report of the Interagency Climate Adaptation Team.
Norby, R.J., O'Neill, E.G., Luxmoore, R.J., 1986. Effects of Atmospheric CO2 Enrichment on the Growth and Mineral Nutrition of Quercus alba Seedlings in Nutrient-Poor soil ,. Plant Physiology 83–89.
Nosanchuk, J.D., Stark, R.E., Casadevall, A., 2015. Fungal melanin: What do we know about structure? Frontiers in Microbiology 6, 1–7.
Ontl, T. A. & Schulte, L. A., 2012. Soil Carbon Storage. Nature Education Knowledge 3(10):35
Pellitier, P.T., Zak, D.R., 2017. Ectomycorrhizal fungi and the enzymatic liberation of nitrogen from soil organic matter: why evolutionary history matters. New Phytologist 217, 68–73.
Pierce, J.A., Rast, D.M., 1995. A comparison of native and synthetic mushroom melanins by Fourier-transofm infrared spectroscopy. Phytochemistry 39, 49–55.
Post, W.M., Kwon, K.., 2000. Soil carbon sequestration and land-use change : processes and potential. Global Change Biology 6, 317–327.
Prados-Rosales, R., Toriola, S., Nakouzi, A., Chatterjee, S., Stark, R., Gerfen, G., Tumpowsky, P., Dadachova, E., Casadevall, A., 2015. Structural characterization of melanin pigments from commercial preparations of the edible mushroom Auricularia auricula. Journal of Agricultural and Food Chemistry 63, 7326–7332.
Rillig, M.C., Treseder, K.K., Allen, M.F., 2002. Global Change and Mycorrhizal Fungi, in: Mycorrhizal Ecology. pp. 135–162.
Schlesinger, W.H., Bernhardt, E.S., 2013. The Global Carbon Cycle. Biogeochemistry 419–444.
Schmidt, M.W.I., Torn, M.S., Abiven, S., Dittmar, T., Guggenberger, G., Janssens, I.A., Kleber, M., Kögel-Knabner, I., Lehmann, J., Manning, D.A.C., Nannipieri, P., Rasse, D.P., Weiner, S., Trumbore, S.E., 2011. Persistence of soil organic matter as an ecosystem property. Nature 478, 49–56.
Schreiner, K., Blair, N., Egerton-Warburton, L., Levinson, W., 2014. Contribution of Fungal Macromolecules to Soil Carbon Sequestration.
Shah, F., Nicolás, C., Bentzer, J., Ellström, M., Smits, M., Rineau, F., Canbäck, B., Floudas, D., Carleer, R., Lackner, G., Braesel, J., Hoffmeister, D., Henrissat, B., Ahrén, D., Johansson, T., Hibbett, D.S., Martin, F., Persson, P., Tunlid, A., 2016. Ectomycorrhizal fungi decompose soil organic matter using oxidative mechanisms adapted from saprotrophic ancestors. New Phytologist 209, 1705–1719.
Simpson, A.J., Simpson, M.J., Smith, E., Kelleher, B.P., 2007. Microbially derived inputs to soil organic matter: Are current estimates too low? Environmental Science and Technology 41, 8070–8076.
Six, J., Conant, R.T., Paul, E.A., Paustian, K., 2002. Stabilization mechanisms of soil organic matter : Implications for C-saturation of soils 155–176.
Six, J., Frey, S.D., Thiet, R.K., Batten, K.M., 2006. Bacterial and Fungal Contributions to Carbon Sequestration in Agroecosystems. Soil Science Society of America Journal

70, 555–569.
Smiderle, F.R., Olsen, L.M., Ruthes, A.C., Czelusniak, P.A., Sassaki, G.L., Gorin, P.A.J., Iacomini, M., 2012. Exopolysaccharides , proteins and lipids in Pleurotus pulmonarius submerged culture using different carbon sources. Carbohydrate Polymers 87, 368–376.
Stankiewicz, B.A., Mastalerz, M., Hof, C.H.J., Evershed, R.P., 1998. Biodegradation of the chitin-protein complex in crustacean cuticle. Organic Geochemistry 28, 67–76.
Swift, M.J., Heal, O.W., Anderson, J.M., 1979. Decomposition in Terres- trial Ecosystems. Blackwell, Oxford.
Taylor, B.R., Parkinson, D., Parsons, W.F.J., 1989. Nitrogen and Lignin Content as Predictors of Litter Decay Rates : A Microcosm Test: Barry R . Taylor , Dennis Parkinson and William F . J . Parsons Published by : Wiley on behalf of the Ecological Society of America Stable Ecology 70, 97–104.
Tian, S., Garcia-rivera, J., Yan, B., Casadevall, A., Stark, R.E., 2003. Accelerated Publications Unlocking the Molecular Structure of Fungal Melanin Using 13 C Biosynthetic. Society 42, 27–31.
Tunlid, A., Lindahl, B.D., 2015. Tansley insight Ectomycorrhizal fungi – potential organic matter decomposers , yet not saprotrophs 1443–1447.
Wakamatsu, K., Ito, S., 2002. Review : Innovative Technology Advanced Chemical Methods in Melanin Determination 174–183.
Westrich, J.T., Berner, R.A., 1984. The role of sedimentary organic matter in bacterial sulfate reduction : The G model tested ’ 29, 236–249.
Wickings, K., Grandy, A.S., Reed, S.C., Cleveland, C.C., 2012. The origin of litter chemical complexity during decomposition. Ecology Letters 1180–1188.
Wildung, R.E., Garland, T.R., Buschbom, R.L., 1975. The interdependent effects of soil temperature and water content on soil respiration rate and plant root decomposition in arid grassland soils. Soil Biology and Biochemistry 7, 373–378.
Zhong, J., Frases, S., Wang, H., Casadevall, A., Stark, R.E., 2008. Following fungal melanin biosynthesis with solid-state NMR: Biopolymer molecular structures and possible connections to cell-wall polysaccharides. Biochemistry 47, 4701–4710.